Anatomical connectivity along the anterior-posterior axis of the human hippocampus: new insights using quantitative fibre-tracking.

Marshall A. Dalton[1,2]*, Arkiev D'Souza[2], Jinglei Lv[1,2], Fernando Calamante[1,2,3].

[1] School of Biomedical Engineering, Faculty of Engineering, The University of Sydney, Sydney, New South Wales, Australia, 2050

[2] Brain and Mind Centre, The University of Sydney, Sydney, New South Wales, Australia, 2050

[3] Sydney Imaging, The University of Sydney, Sydney, New South Wales, Australia, 2050

***Corresponding Author**

Marshall Dalton. Brain and Mind Centre, The University of Sydney, 94 Mallett St, Camperdown, NSW, Australia, 2050.

Email: marshall.dalton@sydney.edu.au

Keywords: Hippocampus, Diffusion-Weighted Imaging, Track-Weighted Imaging, Hippocampal Subfields, Structural Connectivity.

Abstract

The hippocampus supports multiple cognitive functions including episodic memory. Recent work has highlighted functional differences along the anterior-posterior axis of the human hippocampus but the neuroanatomical underpinnings of these differences remain unclear. We leveraged track-density imaging to systematically examine anatomical connectivity between the cortical mantle and the anterior-posterior axis of the *in-vivo* human hippocampus. We first identified the most highly connected cortical areas and detailed the degree to which they preferentially connect along the anterior-posterior axis of the hippocampus. Then, using a tractography pipeline specifically tailored to measure the location and density of streamline endpoints within the hippocampus, we characterised where, within the hippocampus, these cortical areas preferentially connect. Our results were striking in showing that different parts of the hippocampus preferentially connect with distinct cortical areas. Furthermore, we provide evidence that both gradients and circumscribed areas of dense extrinsic anatomical connectivity exist within the human hippocampus. These findings inform conceptual debates in the field by unveiling how specific regions along the anterior-posterior axis of the hippocampus are associated with different cortical inputs/outputs. Overall, our results represent a major advance in our ability to map the anatomical connectivity of the human hippocampus *in-vivo and* inform our understanding of the neural architecture of hippocampal dependent memory systems in the human brain. This detailed characterization of how specific portions of the hippocampus anatomically connect with cortical brain regions may promote a better understanding of its role in cognition and we emphasize the importance of considering the hippocampus as a heterogeneous structure.

Introduction

There is long-standing agreement that the hippocampus is essential for supporting episodic long-term memory (1) and for facilitating spatial navigation (2). The hippocampus has more recently been linked with other roles including imagination of fictitious and future experiences (3, 4), visuospatial mental imagery (5), visual perception (6, 7) and decision making (8). It is a complex structure containing multiple subregions (referred to as subfields) including the dentate gyrus (DG), cornu ammonis (CA) 4-1, subiculum, presubiculum and parasubiculum. Accumulating evidence suggests that different hippocampal subfields are preferentially recruited during different cognitive functions (5, 9). Functional differences are also present along the anterior-posterior axis of the hippocampus (10-15) and its subfields (16, 17). Despite recent advances in understanding functional differentiation within the hippocampus, much less is known about the neuroanatomical underpinnings of these functional differences in the human brain. A more detailed understanding of anatomical connectivity along the anterior-posterior axis of the human hippocampus is needed to better understand and interpret these functional differences.

Much of our knowledge regarding the anatomical connectivity of the human hippocampus is inferred from the results of tract-tracing studies in rodent and non-human primate brains. While this information has been fundamental to inform theoretical models of hippocampal-dependent memory function, recent investigations have highlighted potential differences between connectivity of the human and non-human primate hippocampus (18). This suggests that, in addition to evolutionarily conserved patterns of hippocampal connectivity, human and non-human primates may also have unique patterns of connectivity. More detailed characterisations of human hippocampal connectivity are, therefore, essential to advance our understanding of the neural architecture that underpins hippocampal dependent memory and cognition in the human brain.

Tract-tracing studies in rodents and non-human primates have revealed that the hippocampus is highly connected with multiple cortical areas. It is well established that the entorhinal cortex (EC) is the primary interface between the hippocampus and multiple brain regions (19). Other medial temporal lobe (MTL) structures including the perirhinal (PeEc) and posterior parahippocampal (PHC) cortices also have direct anatomical connections with the hippocampus (20-23) albeit to a lesser degree. However, direct cortico-hippocampal pathways are not confined to MTL cortices. Anterograde and retrograde labelling studies in non-human primates have revealed direct and reciprocal connections between the hippocampus and multiple cortical areas in temporal (21, 24), parietal (25, 26) and frontal (27, 28) lobes. These detailed investigations show that specific cortical areas preferentially connect with circumscribed portions along the anterior-posterior axis of hippocampal subfields. For example, retrograde labelling studies in the macaque reveal that the retrosplenial cortex (RSC) in the parietal lobe has direct connectivity with posterior portions of the presubiculum while area TE in the inferior temporal lobe displays preferential connectivity with posterior portions of the CA1/subiculum transition area (22). While patterns of cortico-hippocampal connectivity such as these have been observed in the non-human primate brain, we know less about these patterns in the human brain.

Detailed examination of structural connectivity (SC) of the human hippocampus has been difficult to pursue mainly due to the technical difficulties inherent to probing hippocampal connectivity *in-vivo* using MRI. Limitations in both image resolution and fibre tracking methods have precluded our ability to probe cortico-hippocampal pathways in a sufficient level of detail. Some researchers have partially circumvented these constraints by investigating blocks of ex-vivo MTL tissue using high-field MRI scanners (29-31) or novel methods such as polarised light microscopy (18). While these studies have provided important insights relating to MTL-hippocampal pathways, we have less knowledge regarding how the human hippocampus connects with more distant cortical areas. Detailed characterisations of anatomical connectivity between the hippocampal long-axis and broader cortical networks are needed to better understand functional heterogeneity within the hippocampus (32).

Of the extant *in-vivo* MRI studies that have examined SC of the human hippocampus, several have focussed on connectivity between the hippocampus and specific cortical or subcortical areas (33-37) with a primary focus on disease states. To our knowledge, only one study has attempted to characterise the broader hippocampal 'connectome' in the healthy human brain. Maller and colleagues (38) used diffusion MRI (dMRI) data with multiple diffusion strengths and high angular resolution combined with

track density imaging (TDI) to characterise SC between the whole hippocampus and cortical and subcortical brain regions. A quantitative analysis of streamline numbers (as a surrogate measure of connectivity) seeded from the whole hippocampus showed that the most highly connected brain regions were the temporal lobe followed by subcortical, occipital, frontal and parietal regions. The primary focus of their study, however, was a description of six dominant white matter pathways that accounted for most cortical and subcortical streamlines connecting with the whole hippocampus. Together, these studies have provided an important glimpse into the complexity of human hippocampal SC but important gaps in our knowledge remain. Specifically, there has been no systematic examination of SC between the cortical mantle and the anterior-posterior axis of the human hippocampus and we do not know where, within the hippocampus, specific cortical areas preferentially connect.

In the current study, we aimed to systematically examine patterns of SC between cortical brain areas and the anterior-posterior axis of the human hippocampus. We combined high-quality dMRI data from the Human Connectome Project (HCP), cutting-edge quantitative fibre-tracking methods, and a processing pipeline specifically tailored to study hippocampal connectivity with three primary aims; (i) to quantitatively characterise SC between the cortical mantle (focused on non-MTL areas) and the whole hippocampus; (ii) to quantitatively characterise how SC varies between cortical areas and the head, body and tail of the hippocampus and (iii) to use TDI combined with 'endpoint density mapping' to quantitatively assess, visualise and map the spatial distribution of streamline endpoints within the hippocampus associated with each cortical area.

Our results represent a major advance in; (i) our ability to map the anatomical connectivity of the human hippocampus *in-vivo* and; (ii) our understanding of the neural architecture that underpins hippocampal dependent memory systems in the human brain. We provide fundamental insights into how specific cortical areas preferentially connect along the anterior-posterior axis of the hippocampus and identify where streamlines associated with a given cortical area preferentially connect within the hippocampus. These detailed anatomical insights will help fine-tune network connectivity models and will have an impact on current theoretical models of human hippocampal memory function[1].

[1] A preliminary version of this work was presented at the 30th Annual Meeting of the International Society for Magnetic Resonance in Medicine (May 17, 2021).

Results

We first characterised SC between the whole hippocampus and all cortical areas of the HCP Multi-Modal Parcellation (HCPMMP) (39). The primary focus of this study was SC between the hippocampus and non-MTL cortical areas. We therefore focus on cortical areas outside of the MTL (information relating to MTL cortices are presented in Supplementary Materials Note S1, Supplementary Figures S1 and S2 and Supplementary Tables S1 and S2).

Which specific cortical areas most strongly connect with the whole hippocampus?

For brevity, we present results relating to the twenty cortical areas with the highest degree of SC with the whole hippocampus. The hippocampus displayed the highest degree of SC with discrete cortical areas in temporopolar (areas TGv, TGd; abbreviations for all cortical areas are defined in Supplementary Table S3), inferolateral temporal (areas TF, TE2a, TE2p), medial parietal (areas RSC, ProS, POS1, POS2, DVT) dorsal and ventral stream visual (areas V3A, V6, FFC, VVC, VMV1, VMV2) and early visual (occipital) cortices (areas V1, V2, V3, V4). Results are summarised in Figure 1a and Table 1 lists each cortical area and their associated strength of connectivity with the whole hippocampus. A full list of all cortical areas of the HCPMMP and their associated strengths of connectivity are provided in Supplementary Table S1.

Do cortical areas display preferential connectivity along the anterior-posterior axis of the hippocampus?

Next, we conducted a more detailed characterisation of SC between each cortical area and the head, body and tail portions of the hippocampus. For brevity, we present results relating to the twenty most highly connected cortical areas described above. Results are summarised in Figure 1b and Table 2 which lists each cortical area, their associated strength of connectivity with the head, body and tail portions of the hippocampus and the results of statistical analyses (Bonferroni corrected paired-samples t-tests; see Methods). A full list of all cortical areas and their associated strengths of connectivity with the head, body and tail portions of the hippocampus are provided in Supplementary Table S2.

Each of the twenty most highly connected cortical areas displayed preferential connectivity with specific regions along the anterior-posterior axis of the hippocampus. These can be categorised into four distinct patterns: 1. an anterior-to-posterior gradient of increasing connectivity; 2. a posterior connectivity bias; 3. an anterior connectivity bias; and 4. a body connectivity bias.

Eight of the twenty most highly connected cortical areas displayed a gradient of increasing connectivity from the head-to-tail of the hippocampus. These were area ProS, V1, V2, V3, DVT, V4, V6 and V3A (abbreviations are defined in Supplementary Table S3). The results of Bonferroni corrected paired-samples t-tests revealed that these regions each showed a statistically significant difference in connectivity strength between the head and body, the body and tail and the head and tail portions of the hippocampus (see Figure 1b and Table 2). That is, each of these cortical areas displayed the lowest connectivity with the hippocampal head, significantly increased connectivity with the body and the strongest connectivity with the tail.

Five areas had significantly stronger connectivity with the posterior 2/3 of the hippocampus. These were area POS1, VMV1, VMV2, RSC and POS2. The results of Bonferroni corrected paired-samples t-tests revealed that these cortical areas displayed a high degree of connectivity with the body and tail of the hippocampus (no statistically significant difference in connectivity) and significantly lower connectivity with the hippocampal head (see Figure 1b and Table 2).

Three of the twenty most highly connected cortical areas had significantly greater connectivity with the anterior 2/3 of the hippocampus These were area TF, TGd and TGv. The results of Bonferroni corrected paired-samples t-tests revealed that these cortical areas displayed a high degree of connectivity with

the head and body of the hippocampus (no statistically significant difference in connectivity) and significantly lower connectivity with the tail of the hippocampus (see Figure 1b and Table 2).

Four areas had greater connectivity with the body of the hippocampus. These areas were TE2a, VVC, FFC and TE2p. The results of Bonferroni corrected paired-samples t-tests revealed that these areas showed statistically significant differences in connectivity strength between the head and body of the hippocampus. TE2a, VVC and TE2p showed statistically significant differences in connectivity strength between the body and tail portions but FFC did not (following Bonferroni correction). TE2a also showed a statistically significant difference between the head and tail portions of the hippocampus but VVC, FFC and TE2p did not (see Figure 1b and Table 2). That is, each of these cortical areas displayed the highest degree of connectivity with the body of the hippocampus.

To summarise, our results detail the degree to which specific cortical areas preferentially connect along the anterior-posterior axis of the hippocampus. While some cortical areas displayed gradients of connectivity strength along the anterior-posterior axis of the hippocampus, others displayed preferential connectivity with specific portions of the hippocampus.

Do cortical areas display unique distributions of endpoint density within the hippocampus?

Our tractography pipeline was specifically tailored to allow streamlines to enter/leave the hippocampus and quantitatively measure the location and density of streamline endpoints within the hippocampus using TDI. We created endpoint density maps (EDMs) that allowed us to visualise the spatial distribution of hippocampal endpoint density associated with each cortical area (described in Methods). While it is not feasible to present the results for all cortical areas of the HCPMMP, we describe results for the twenty most highly connected cortical areas described above.

The results of group level analyses confirmed that specific cortical areas preferentially connect with different regions within the human hippocampus. For example, areas in the medial parietal cortex (ProS, POS1, RSC, DVT, POS2) displayed high endpoint density primarily in medial portions of the posterior hippocampus (see yellow arrows in Figure 2a for a representative example of endpoint densities associated with RSC; see Supplementary Figure S3 for other areas). In contrast, areas in temporopolar and inferolateral temporal cortex (TF, TGd, TGv, TE2a, TE2p) displayed high endpoint density primarily along the lateral aspect of the anterior 2/3 of the hippocampus and in a circumscribed region of the anterior medial hippocampus (see blue and white arrows respectively in Figure 2b for a representative example of endpoint densities associated with TGv; see Supplementary Figure S4 for other areas). Similar to areas in the medial parietal cortex, areas in the occipital cortices (V1-4, V6, V3a) displayed high endpoint density primarily in the posterior medial hippocampus and, to a lesser degree, in a circumscribed region of the anterior medial hippocampus (see yellow and white arrows respectively in Figure 2c for endpoint densities associated with V1; see Supplementary Figure S5 for other areas).

In parallel with these differences, specific regions within the hippocampus displayed high endpoint density for multiple cortical areas. For example, several medial parietal and occipital cortical areas displayed high endpoint density in the posterior medial hippocampus (yellow arrows in Supplementary Figures S3 and S5). In contrast, several cortical areas in the temporal pole and inferolateral temporal lobe displayed high endpoint density in the anterior lateral hippocampus (blue arrows Supplementary Figure S4). Another cluster of high endpoint density in the anterior medial hippocampus (at the level of the uncal apex) was more broadly associated with specific areas in temporal, medial parietal and occipital cortices (white arrows in Supplementary Figures S3-5).

To further probe hippocampal endpoint density common to these cortical regions, we averaged the EDMs for anatomically related cortical areas. For example, we averaged the EDMs of the five most highly connected cortical areas in the temporal lobe (TF, TGd, TGv, TE2a, TE2p) and observed high endpoint density common to these areas was more clearly localised along the anterior lateral hippocampus and in a circumscribed region of the anterior medial hippocampus (blue and white arrows respectively in Figure 3a). Likewise, when we averaged the most highly connected cortical areas in the medial parietal and occipital cortices respectively, high endpoint density common to each of these areas was localised in the posterior medial hippocampus and, to a lesser degree, in a circumscribed region

of the anterior medial hippocampus (Yellow and white arrows respectively in Figure 3b and 3c). When we averaged the EDMs across all of these areas, high endpoint density common to this broader collection was localised to separate circumscribed clusters in the posterior and anterior medial hippocampus (yellow and white arrows respectively in Figure 3d) and in punctate clusters along the anterior-posterior extent of the lateral hippocampus (blue arrows in Figure 3d). Our results suggest that these specific regions within the hippocampus are highly connected with multiple cortical areas in medial parietal, temporal and occipital lobes.

In addition, our novel method allowed us to isolate and visualise streamlines between specific cortical areas and the hippocampus and map the spatial distribution of hippocampal endpoint density at the single participant level. Representative examples are presented in Figure 4. Figure 4b displays isolated streamlines associated with areas TF and V1 in a single participant. Figure 4d displays the hippocampal EDMs associated with each of these cortical areas in the same participant. When overlaid on the T1-weighted image, EDMs resemble histological staining of post-mortem tissue, albeit *in-vivo* and at a coarser level of detail (see bottom panels of Figure 4d). For example, for area TF, in a coronal slice taken at the uncal apex (red line) endpoint density was primarily localised to specific areas in the medial hippocampus (red panel). For area V1, in a coronal slice taken at the hippocampal tail (turquoise line) endpoint density was also localised to the medial hippocampus (turquoise panel). When compared with equivalent sections of histologically stained tissue, the location of these clusters of endpoint density roughly align with the location of the distal subiculum/proximal presubiculum for both TF and V1 (indicated by black arrows; see also Figure 5a). The location of endpoint density associated with each cortical area was broadly consistent across participants (evidenced by the results of our group level analyses). A detailed examination of individual variability in these patterns, however, was beyond the scope of the current investigation and will be addressed in future studies.

Discussion

This study represents a comprehensive *in-vivo* characterisation of SC between cortical brain areas and the human hippocampus. We identified cortical areas with the highest degree of SC with the whole hippocampus, measured the degree to which these cortical areas preferentially connect along the anterior-posterior axis of the hippocampus, and deployed a tailored method to characterise where, within the hippocampus, each cortical area preferentially connects. Our results reveal how specific cortical areas preferentially connect with circumscribed regions along the anterior-posterior and medial-lateral axes of the hippocampus. Our results broadly reflect observations from the non-human primate literature (discussed below) and contribute new neuroanatomical insights to inform debates on human hippocampal function as it relates to its anterior-posterior axis. This work represents an important advance in our understanding of the neural architecture that underpins hippocampal dependent memory systems in the human brain. In addition, our method represents a novel approach to conduct detailed *in-vivo* investigations of the anatomical connectivity of the human hippocampus with implications for basic and clinical neuroscience.

Preliminary whole hippocampus and anterior-posterior axis analyses

First, we consider the preliminary whole hippocampus analysis. Aligning with our predictions, the hippocampus was most strongly connected with the EC and highly connected with surrounding MTL structures (See Supplementary Materials for further information relating to MTL structures). Beyond the MTL, specific cortical areas in temporopolar, inferotemporal, medial parietal and occipital cortices displayed the highest degree of SC with the hippocampus. These results broadly align with recent DWI investigations that reported SC between the whole hippocampus and these cortical regions in the human brain (38). Our anterior-posterior axis analyses provided a more detailed quantitative characterisation of cortico-hippocampal SC by measuring the degree to which specific cortical areas preferentially connect along the anterior-posterior axis of the hippocampus. In brief, specific areas within temporopolar and inferolateral temporal cortices displayed preferential SC with the head and/or body of the hippocampus. In contrast, medial parietal and occipital cortical areas displayed a posterior hippocampal connectivity bias most strongly with the hippocampal tail. These patterns of SC mirror

commonly observed functional links between the anterior hippocampus and temporal regions and between the posterior hippocampus and parietal/occipital regions (16, 40-43). Our results provide new insights into the neuroanatomical architecture of these functional associations in the human brain. Further interpretation of these observations are facilitated by the results of our more detailed endpoint density analyses and are discussed below.

Endpoint density mapping of human cortico-hippocampal connectivity

To date, our knowledge of human cortico-hippocampal anatomical connectivity is largely inferred from the results of tract-tracing studies conducted in non-human primates and rodents. We know much less about these patterns in the human brain. To address this gap, we adapted a tractography pipeline to track streamlines entering/leaving the hippocampus, identify the location of their 'endpoints' and create spatial distribution maps of endpoint density within the hippocampus associated with each cortical area. The resulting EDMs allowed us to quantitatively assess and visualise where, within the hippocampus, different cortical areas preferentially 'connect'. To our knowledge, this is the first time such a specific approach has been used to map anatomical connectivity of the human hippocampus *in-vivo*.

We observed striking differences in the location of endpoint density along both the anterior-posterior and medial-lateral axes of the hippocampus. For example, temporopolar and inferolateral temporal cortical areas displayed the greatest endpoint density along the lateral aspect of the head and body of the hippocampus (Supplementary Figure S4a-e; aligning with the location of distal CA1/proximal subiculum; see Figure 5a) and in a circumscribed cluster in the anterior medial hippocampus at the level of the uncal apex (Supplementary Figure S4a-d; aligning with the location of distal subiculum/proximal presubiculum; see Figure 5a). In contrast, areas in the medial parietal and occipital cortices displayed the greatest endpoint density along the medial aspect of the tail and body of the hippocampus (Supplementary Figures S3a-e (medial parietal) and 5a-e (occipital); aligning with the location of the distal subiculum/proximal presubiculum; see Figure 5a). We discuss these observations in relation to the non-human primate literature below.

Comparison to tract-tracing data in non-human primates

The results of our endpoint density analyses broadly overlap with observations from the non-human primate literature. For simplicity, we demonstrate this by comparing the results for three cortical areas with equivalent observations from the series of tract-tracing investigations of the macaque hippocampus described by Insausti & Muñoz (22). In the macaque, retrograde tracer injection into the RSC results in localised labelling of cells in the posterior presubiculum. Our results revealed high endpoint densities associated with the RSC were primarily localised to a homologous region in the posterior medial hippocampus (distal subiculum/proximal presubiculum; brown ellipsoids in Figure 5b). In the macaque, retrograde tracer injection into the PeEc results in dense labelling of cells along the anterior-posterior axis of the hippocampus primarily localised to the CA1/subiculum transition area and the presubiculum. Our results mirrored this pattern. We observed areas of endpoint density along the lateral hippocampus (blue ellipsoids in Figure 5c; distal CA1/proximal subiculum) and along the medial hippocampus (brown ellipsoids in Figure 5c; distal subiculum/proximal presubiculum). In the macaque, labelling associated with area TE is scarce compared to that of the PeEc with labelled cells localised to the posterior CA1/subiculum transition area and the posterior presubiculum. Again, our results broadly aligned with this pattern. Compared with PeEc, we observed less endpoint density associated with TE2a (roughly corresponding to the injection site described by Insausti & Muñoz) which was primarily localised to the lateral (blue ellipsoids in Figure 5d; distal CA1/proximal subiculum) and medial (brown ellipsoids in Figure 5d; distal subiculum/proximal presubiculum) hippocampus. In contrast to the macaque, however, endpoint density was most strongly expressed in the lateral aspect of the anterior hippocampus (red ellipsoid in Figure 5d). We discuss potential interpretations for this and other differences later in the discussion. Overall, our results broadly aligned with patterns observed in the non-human primate brain and provide new and detailed insights regarding where specific cortical areas preferentially connect within the human hippocampus.

New evidence for hubs of anatomical connectivity in the human hippocampus?

High endpoint density within the hippocampus was restricted to areas that aligned with the location of CA1, subiculum and the pre- and parasubiculum and was notably absent from areas aligning with DG/CA4 (hilus), CA3 and CA2. These observations mirror reports in the rodent and non-human primate literature where non-EC cortical areas predominantly connect with subicular cortices and the CA1/subiculum transition area (20, 22). Indeed, in non-human primates, the CA1/subiculum transition area and the presubiculum appear to be 'hotspots' of anatomical connectivity for multiple cortical areas (22, 44). In accordance with this, we observed that these specific regions within the human hippocampus displayed high endpoint density for multiple cortical areas. For example, the anterior lateral hippocampus (aligning with the distal CA1/proximal subiculum) displayed high endpoint density for multiple temporal cortical areas (Figure 3a) and the posterior medial hippocampus (aligning with the distal subiculum/proximal presubiculum) displayed high endpoint density for multiple areas of the medial parietal and occipital cortices (Figure 3b and c respectively). Another cluster of high endpoint density in the anterior medial hippocampus (aligning with the distal subiculum/proximal presubiculum) was more broadly associated with temporal, medial parietal and occipital areas (Figure 3a-d). Taken together, these observations provide evidence that discrete hubs of dense anatomical connectivity may exist along the anterior-posterior axis of the human hippocampus and that these hubs align with the location of the CA1/subiculum transition area and the distal subiculum/proximal presubiculum.

To the best of our knowledge, this is the first quantitative report of these patterns in the human brain and we highlight the intriguing possibility that two medial hippocampal hubs of high anatomical connectivity may exist; a posterior medial hub preferentially linked with visuospatial processing areas in medial parietal and occipital cortices and an anterior medial hub more broadly linked with temporopolar, inferotemporal, medial parietal and occipital areas. We tentatively speculate that these circumscribed areas of the medial hippocampus could represent highly connected hubs of information flow between the hippocampus and distributed cortical networks. Indeed, the cortical areas identified in this study may represent key areas for direct cortico-hippocampal interactions in support of episodic/semantic memory processing and consolidation.

Accumulating evidence from neuroimaging and clinical studies suggest that the medial hippocampus plays an important role in visuospatial cognition. The anterior medial hippocampus is consistently engaged during cognitive tasks that require processing of naturalistic scene stimuli in aid of episodic memory (45), visuospatial mental imagery (5), perception and mental construction (e.g., imagination) of scenes (46, 47). Strikingly, the location of the anterior medial cluster of anatomical connectivity observed in the current study aligns with the location of functional clusters commonly observed in functional MRI investigations of these cognitive processes (5, 45-48) (see Figure 6 for comparison). Furthermore, recent evidence from the clinical domain suggests that the posterior medial hippocampus may be a critical hub in a broader memory circuit (49). The medial hippocampus has more broadly been proposed as a putative hippocampal hub for visuospatial cognition (50). Our results lend further support to these proposals by showing that specific regions of both the anterior and posterior medial hippocampus display dense anatomical connectivity with multiple cortical areas in the human brain.

In addition, our results provide new anatomical insights to inform current debates on functional differentiation along the anterior-posterior axis of the human hippocampus. Our anterior-posterior axis analyses revealed that specific cortical areas displayed a gradient style increase in connectivity strength along the anterior-posterior axis of the hippocampus while others displayed non-linear patterns of connectivity. In parallel, the results of our endpoint density analyses suggest that discrete clusters of dense connectivity may also exist within the hippocampus. Together, these observations provide new evidence to support recent proposals that both gradients and circumscribed parcels of extrinsic connectivity may exist along the anterior-posterior axis of the human hippocampus (13-15) and that different circuits may exist within the hippocampus, each associated with different cortical inputs that underpin specific cognitive functions (5). How the complex patterns of anatomical connectivity observed in the current study relate to functional differentiation along the long-axis of the hippocampus (11-14) and it's subfields (16, 17) will be a fruitful area of research in coming years.

Are there human specific patterns of cortico-hippocampal connectivity?

Despite areas of concordance with the non-human primate literature noted above, we also observed important differences. As noted earlier, we observed broader patterns of endpoint density for area TE2a than we expected based on the non-human primate literature. Also, non-human primate studies have found direct and substantial connectivity between the hippocampus and orbitofrontal and superior temporal cortices (22). We found only weak patterns of connectivity between the hippocampus and these regions. Also of note, in contrast to the non-human primate literature, we observed dense patterns of anatomical connectivity between the posterior medial hippocampus and early visual processing areas in the occipital lobe. It is important to note that our methods differ significantly from the carefully controlled injection of tracer into circumscribed portions of the brain. MRI investigations of SC are inherently less precise, and methodological limitations likely explain some of our observed differences. It is important to note, however, that while we expect to see evolutionarily conserved overlaps in SC between macaque and human brains, we should not expect exactly the same patterns of connectivity. Since splitting from a common ancestor, macaques and humans have likely evolved species specific patterns of cortico-hippocampal connectivity to support species specific cognitive functions. Whether differences observed in the current study reflect methodological limitations, species differences or perhaps most likely, a mix of both, require further investigation.

To our knowledge, only one prior study has attempted to characterise the broader hippocampal 'connectome' in the healthy human brain (38). Our study differs from this recent report in several important technical aspects. We analysed connectivity profiles of the head, body and tail portions of the hippocampus separately in addition to the whole hippocampus. We manually delineated the hippocampus for each participant to ensure full coverage of the hippocampus and to minimise the hippocampus mask 'spilling' into adjacent white matter (a common occurrence with automated segmentation methods; see Supplementary Figure S6). We used the HCPMMP scheme, which provides more detailed subdivisions of cortical grey matter (39). We also included SIFT2 (51) in our analysis pipeline to increase biological accuracy of quantitative connectivity estimates. Finally, we used a carefully adapted tractography method that incorporates anatomical constraints and allowed streamlines to enter/leave the hippocampus, which provided us with a means to determine the location and topography of streamline 'endpoints', and therefore their distribution within the hippocampus (see Methods for detail relating to each of these points).

In closing, this study represents a first attempt to apply this method and has some limitations. Specifically, our method relies on several manual steps to delineate the hippocampus and to amend the grey matter-white matter interface that abuts the inferior portion of the hippocampus (described in Materials and Methods). This can be time consuming and requires expertise to accurately identify the hippocampus along its entire anterior-posterior extent on structural MRI scans. However, considering automated methods of hippocampal segmentation are sometimes not sufficiently accurate, particularly in the anterior and posterior most extents of the hippocampus (see Supplementary Figure S6 for representative examples), manual delineation is the gold standard and ensures the best results. We restricted our analysis to a limited number of subjects under the age of 35 and selected participants whose hippocampus was clearly visible along its entire anterior-posterior axis on T1-weighted structural scans. While this ensured we used the best data quality available, further work should explore how these results may differ in the context of healthy ageing and in diseases that affect the hippocampus such as Alzheimers disease, epilepsy and schizophrenia. How reliable our pipeline is in data acquired with more traditional clinical protocols remains to be explored and was beyond the scope of the current study. Despite the high-quality HCP data used in this study, limitations in spatial resolution likely restrict our ability to track particularly convoluted white-matter pathways within the hippocampus and our results should be interpreted with this in mind. Future work using higher resolution data will allow more targeted investigations and is necessary to confirm or refute the patterns we observed here. These limitations notwithstanding, our results provide new detailed insights into anatomical connectivity of the human hippocampus, can inform theoretical models of human hippocampal function as they relate to the long-axis of the hippocampus and can help fine-tune network connectivity models.

From a clinical perspective, the hippocampus is central to several neurodegenerative and neuropsychiatric disorders. Considering healthy memory function is dependent upon the integrity of

white-matter fibres that connect the hippocampus with the rest of the brain, developing a more detailed understanding of the anatomical connectivity of the anterior-posterior axis of the hippocampus and its subfields has downstream potential to help us better understand hippocampal-dependent memory decline in ageing and clinical populations. Our novel method can potentially be harnessed to measure changes in anatomical connectivity between the hippocampus and cortical areas known to be affected in neurodegenerative diseases, to assist with monitoring of disease progression and/or as a diagnostic tool. In addition, our method could be deployed to visualise patient specific patterns of hippocampal connectivity to support surgical planning in patients who require MTL resection for intractable MTL epilepsy.

Materials and Methods

Participant details

Ten subjects (7 female) were selected from the minimally processed Human Connectome Project (HCP) 100 unrelated subject database (<35yo). Subjects were selected based on the scan quality and visibility of the outer boundaries of the hippocampus on each participants T1-weighted structural MRI scan. This was done in order to increase the anatomical accuracy of our hippocampal segmentations (described below).

Image acquisition

The HCP diffusion protocol consisted of three diffusion-weighted shells (b-values: 1000, 2000 and 3000 s/mm2, with 90 diffusion weighting directions in each shell) plus 18 reference volumes (b = 0 s/mm2). Each diffusion-weighted image was acquired twice, with opposite phase-encoded direction to correct for image distortion (52). The diffusion image matrix was 145 × 145 with 174 slices and an isotropic voxel size of 1.25 mm. The TR and TE were 5520 and 89.5 ms, respectively. Each subject also included a high resolution T1-weighted dataset, which was acquired with an isotropic voxel size of 0.7 mm, TR/TE = 2400/2.14 ms, and flip angle = 8°.

Manual segmentation of the hippocampus

The whole hippocampus was manually segmented for each participant on coronal slices of the T1-weighted image using ITK-SNAP (53). Although automated methods of hippocampal segmentation are available, they are sometimes not sufficiently accurate particularly in the anterior and posterior most extents of the hippocampus (see Supplementary Figure S6 for representative examples). Although labour intensive, manual segmentation by an expert in hippocampal anatomy remains the gold-standard for detailed and accurate investigation of the human hippocampus. We adapted the manual segmentation protocol outlined by Dalton and colleagues (54). While this protocol details a method for segmenting hippocampal subfields, we followed guidelines as they relate to the outer boundaries of the hippocampus. This ensured that the whole hippocampus mask for each participant contained all hippocampal subfields (dentate gyrus, CA4-1, subiculum, presubiculum and parasubiculum) and encompassed the entire anterior-posterior extent of the hippocampus (see (54) for details). Representative examples of the hippocampus mask are presented in Supplementary Figures S6 and S7. Manual segmentations were conducted by an expert in human hippocampal anatomy and MRI investigation of the human hippocampus (M. A. D) with 14 years experience including histological (55) and MRI investigations (5, 16, 17, 54). For the anterior-posterior axis analysis, we split each participants whole hippocampus mask into thirds corresponding with the head, body and tail of the hippocampus. This was done in accordance with commonly used anatomical landmark-based methods. In brief, the demarcation point between the head and body of the hippocampus was the uncal apex (10, 56) and the demarcation point between the body and tail of the hippocampus was the anterior most slice in which the crus of the fornix was fully visible (57, 58).

Image pre-processing and whole-brain tractography

Besides the steps carried out by the HCP team as part of the minimally processed datasets, the additional image processing pipeline included in our analysis is summarised in Supplementary Figure S8a. Processing was performed using the MRtrix software package (http://www.mrtrix.org) (59, 60). Additional processing steps were implemented in accordance with previous work (61) and included bias-field correction (62) as well as multi-shell multi-tissue constrained spherical deconvolution to generate a fibre orientation distribution (FOD) image (63-65). The T1 image was used to generate a 'five-tissue-type' (5TT) image using FSL (66-70); tissue 1 = cortical grey matter, tissue 2 = sub-cortical grey matter, tissue 3 = white matter, tissue 4 = CSF, and tissue 5 = pathological tissue. The FOD image and the 5TT image were used to generate 70 million anatomically constrained tracks (66) using dynamic seeding (71) and the 2nd-order Integration over Fibre Orientation Distributions (iFOD2 (72)) probabilistic fibre-tracking algorithm. The relevant parameters included: 70 million tracks, dynamic seeding, backtracking option specified, FOD cut-off 0.06, minimum track length 5 mm, maximum track length 300 mm, maximum of 1000 attempts per seed.

Hippocampus tractography

We developed a tailored pipeline to track streamlines into the hippocampus. To do this, we first amended the gm-wm interface immediately inferior to the hippocampus. This was necessary because the manually segmented hippocampus mask lay slightly superior to the automatically generated gm-wm interface (see Supplementary Figure S7b; middle image). Pilot testing showed that streamlines terminated when reaching this portion of the gm-wm interface, thereby impeding streamlines from traversing the inferior border of the hippocampus. This was a problem because white matter fibres innervate the hippocampus primarily through this region (and also via the fimbria/fornix) (73). It was, therefore, important to ensure that streamlines could cross the inferior border of the hippocampus mask in a biologically plausible manner. To facilitate this, we created an additional hippocampus mask for each participant that extended inferiorly to encompass portions of the gm-wm border that lay immediately inferior to the hippocampus (see Supplementary Figure S7b; right image). This amended hippocampus mask was labelled as white matter in the modified 5TT image (referred to as m5TT). This served to remove the portion of the gm-wm border immediately inferior to the hippocampus and ensured that streamlines could enter/leave the hippocampus in a biologically plausible manner. Additionally, the original whole hippocampus segmentation was assigned as 5th tissue type in the m5TT image (i.e. where no anatomical priors are applied within the ACT framework in MRtrix; Supplementary Figure S8b). This allowed streamlines to move within the hippocampus.

In summary, amending the erroneous gm-wm border allowed streamlines to traverse hippocampal boundaries in a biologically plausible manner and labelling the manually segmented hippocampus as a 5th tissue type permitted streamlines to move within the hippocampus. Together, this allowed us to follow the course of each streamline within the hippocampus and determine the location of each streamline "endpoint" (described below).

Next, the FOD image was used with the m5TT image to generate an additional 10 million tracks. This set of anatomically constrained tracks (66) were seeded from the manually segmented hippocampus, and iFOD2 was used for fibre tracking(72). The 70 million whole-brain tracks and the 10 million hippocampus tracks were combined, and spherical-deconvolution informed filtering of tractograms 2 (SIFT2 (71)) was used on the combined 80 million track file, thereby assigning a weight to each track and providing biological credence to the connectivity measurements (74). Within the SIFT2 framework, connectivity is then computed not by counting the number of tracks but by the sum of its SIFT2 weights. Tracks (and SIFT2 weights) which had an endpoint in the hippocampus were extracted (referred to here as the 'hippocampus tractogram') and used in both the whole hippocampus and anterior-posterior axis analyses.

Whole hippocampus connectivity

FreeSurfer (75) was used to further process the T1-weighted image. The Human Connectome Project Multi-Modal Parcellation 1.0 (HCPMMP) (39) was mapped to each subject in accordance with previous work (76). The parcellation divided the cerebral cortex into 360 parcels (180 per hemisphere). Importantly, we replaced the automated hippocampus and presubiculum parcels with the manually segmented hippocampus (which included the presubiculum) for greater anatomical accuracy (referred to as 'modified HCPMMP'; Supplementary Figure S8c). The structural connectivity of tracks between the hippocampus and the other parcels was obtained using tracks (and SIFT2 weights) from the hippocampus and the modified HCPMMP (containing the whole-hippocampus segmentation). The strength of connectivity between the hippocampus and every other parcel of the HCPMMP was measured by the sum of the SIFT2 weighted connectivity values (51). For each parcel (cortical area), we combined left and right hemisphere values (i.e., left and right retrosplenial cortex) and report bilateral results.

Anterior-posterior axis connectivity

As described in the manual segmentation section, the whole hippocampus was subsequently divided into thirds (head, body and tail, as shown in Supplementary Figure S8d). For the anterior-posterior axis analyses, each of these three regions were added to the HCPMMP as their own unique parcel. In a similar manner to the whole hippocampus connectivity analysis, the strength of connectivity between each hippocampal region (head, body and tail) and each parcel of the modified HCPMMP was measured by the sum of the SIFT2 weighted connectivity values. To assess whether connectivity values between each cortical brain area and the head, body and tail portions of the hippocampus were statistically significant, we conducted Bonferroni-corrected paired-samples t-tests. These are reported in the main text when significant at a level of $p < 0.05$.

Track Density Image (TDI) maps and endpoint creation

TDI mapping of tracks between the whole-hippocampus and the other parcels

The extracted hippocampus tractogram was used to isolate tracks (and weights) between the whole hippocampus parcel and every other parcel in the modified HCPMMP file. Two different TDI maps (77, 78) were computed for each parcel; a TDI of the hippocampus tractogram, and a TDI map showing only the endpoints of this tractogram. Both TDI maps were constructed at 0.2 mm isotropic resolution. These TDI endpoint maps were used in the group-level analysis described below. Note, we refer to these TDI endpoint maps as 'endpoint density maps' (EDMs) in the main text.

Group level analysis of TDI endpoint maps

Group level hippocampus template and TDI endpoint map registration

We employed the symmetric group-wise normalization method (SyGN) (79) implemented in the ANTs toolbox (http://stnava.github.io/ANTs/) to build a population-specific hippocampus template. Specifically, the cross-correlation metric was used to optimize the boundary agreement among the hippocampi masks of each participant. Then, each individual hippocampus mask was registered to the generated population template with the combined linear and non-linear transformation. For each participant, the transformation parameters were recorded and applied to the TDI endpoint maps which were warped into the template space at a resolution of 0.7 mm isotropic. The group average was then calculated providing a group-level distribution map of endpoint density within the hippocampus for each parcel of interest. EDMs were visualised in mrview (the MRtrix image viewer). Representative images displayed in our figures were visualised with the minimum and maximum intensity scale set at 0 and 0.05 respectively and a minimum and maximum threshold set at 0.02 and 0.5 respectively.

Data availability

We used data from the Human Connectome Project (HCP) 100 unrelated subject database; https://www.humanconnectome.org/study/hcp-young-adult/data-releases. Requests for further information regarding our analysis pipeline should be directed to the corresponding author, Marshall Dalton (marshall.dalton@sydney.edu.au).

Author Contributions

M.A.D. and F.C. conceived the experiment. M.A.D., A.D. and J.L. analyzed the data. M.A.D. wrote the manuscript with input from F.C., A.D. and J.L.

Competing Interest Statement

The authors declare no competing interests.

Acknowledgments

Data were provided by the Human Connectome Project, WU-Minn Consortium (Principal Investigators: David Van Essen and Kamil Ugurbil; 1U54MH091657) funded by the 16 NIH Institutes and Centers that support the NIH Blueprint for Neuroscience Research; and by the McDonnell Center for Systems Neuroscience at Washington University, St. Louis, MO.

We are grateful for the support of the National Health and Medical Research Council of Australia (grant numbers APP1091593 and APP1117724), and the Australian Research Council (grant number DP170101815).

The authors acknowledge the technical assistance provided by the Sydney Informatics Hub and Sydney Imaging, two Core Research Facilities of the University of Sydney, Australia.

References

1. W. B. Scoville, B. Milner, Loss of recent memory after bilateral hippocampal lesions. *J Neurol Neurosurg Psychiatry* 20, 11-21 (1957).
2. E. A. Maguire, R. Nannery, H. J. Spiers, Navigation around London by a taxi driver with bilateral hippocampal lesions. *Brain* 129, 2894-2907 (2006).
3. D. Hassabis, D. Kumaran, E. A. Maguire, Using imagination to understand the neural basis of episodic memory. *J Neurosci* 27, 14365-14374 (2007).
4. D. R. Addis, A. T. Wong, D. L. Schacter, Remembering the past and imagining the future: common and distinct neural substrates during event construction and elaboration. *Neuropsychologia* 45, 1363-1377 (2007).
5. M. A. Dalton, P. Zeidman, C. McCormick, E. A. Maguire, Differentiable Processing of Objects, Associations, and Scenes within the Hippocampus. *J Neurosci* 38, 8146-8159 (2018).
6. C. McCormick, M. A. Dalton, P. Zeidman, E. A. Maguire, Characterising the hippocampal response to perception, construction and complexity. *Cortex* 137, 1-17 (2021).
7. A. C. Lee, L. K. Yeung, M. D. Barense, The hippocampus and visual perception. *Front Hum Neurosci* 6, 91 (2012).
8. C. McCormick, C. R. Rosenthal, T. D. Miller, E. A. Maguire, Hippocampal Damage Increases Deontological Responses during Moral Decision Making. *J Neurosci* 36, 12157-12167 (2016).

9. H. R. Dimsdale-Zucker, M. Ritchey, A. D. Ekstrom, A. P. Yonelinas, C. Ranganath, CA1 and CA3 differentially support spontaneous retrieval of episodic contexts within human hippocampal subfields. *Nat Commun* 9, 294 (2018).
10. J. Poppenk, H. R. Evensmoen, M. Moscovitch, L. Nadel, Long-axis specialization of the human hippocampus. *Trends Cogn Sci* 17, 230-240 (2013).
11. A. Plachti, S. B. Eickhoff, F. Hoffstaedter, K. R. Patil, A. R. Laird, P. T. Fox, K. Amunts, S. Genon, Multimodal Parcellations and Extensive Behavioral Profiling Tackling the Hippocampus Gradient. *Cereb Cortex* 29, 4595-4612 (2019).
12. I. K. Brunec, B. Bellana, J. D. Ozubko, V. Man, J. Robin, Z. X. Liu, C. Grady, R. S. Rosenbaum, G. Winocur, M. D. Barense, M. Moscovitch, Multiple Scales of Representation along the Hippocampal Anteroposterior Axis in Humans. *Curr Biol* 28, 2129-2135 e2126 (2018).
13. I. Przezdzik, M. Faber, G. Fernandez, C. F. Beckmann, K. V. Haak, The functional organisation of the hippocampus along its long axis is gradual and predicts recollection. *Cortex* 119, 324-335 (2019).
14. J. Poppenk, Anatomically guided examination of extrinsic connectivity gradients in the human hippocampus. *Cortex* 128, 312-317 (2020).
15. B. A. Strange, M. P. Witter, E. S. Lein, E. I. Moser, Functional organization of the hippocampal longitudinal axis. *Nat Rev Neurosci* 15, 655-669 (2014).
16. M. A. Dalton, C. McCormick, E. A. Maguire, Differences in functional connectivity along the anterior-posterior axis of human hippocampal subfields. *NeuroImage* 192, 38-51 (2019).
17. M. A. Dalton, C. McCormick, F. De Luca, I. A. Clark, E. A. Maguire, Functional connectivity along the anterior-posterior axis of hippocampal subfields in the ageing human brain. *Hippocampus* 29, 1049-1062 (2019).
18. M. M. Zeineh, N. Palomero-Gallagher, M. Axer, D. Grassel, M. Goubran, A. Wree, R. Woods, K. Amunts, K. Zilles, Direct Visualization and Mapping of the Spatial Course of Fiber Tracts at Microscopic Resolution in the Human Hippocampus. *Cereb Cortex* 27, 1779-1794 (2017).
19. A. D. Garcia, E. A. Buffalo, Anatomy and Function of the Primate Entorhinal Cortex. *Annu Rev Vis Sci* 6, 411-432 (2020).
20. J. P. Aggleton, K. Christiansen, The subiculum: the heart of the extended hippocampal system. *Prog Brain Res* 219, 65-82 (2015).
21. M. Yukie, Connections between the medial temporal cortex and the CA1 subfield of the hippocampal formation in the Japanese monkey (Macaca fuscata). *J Comp Neurol* 423, 282-298 (2000).
22. R. Insausti, M. Munoz, Cortical projections of the non-entorhinal hippocampal formation in the cynomolgus monkey (Macaca fascicularis). *Eur J Neurosci* 14, 435-451 (2001).
23. K. L. Agster, R. D. Burwell, Hippocampal and subicular efferents and afferents of the perirhinal, postrhinal, and entorhinal cortices of the rat. *Behav Brain Res* 254, 50-64 (2013).
24. G. W. Van Hoesen, D. L. Rosene, M. M. Mesulam, Subicular input from temporal cortex in the rhesus monkey. *Science* 205, 608-610 (1979).
25. K. S. Rockland, G. W. Van Hoesen, Some temporal and parietal cortical connections converge in CA1 of the primate hippocampus. *Cereb Cortex* 9, 232-237 (1999).
26. S. L. Ding, G. Van Hoesen, K. S. Rockland, Inferior parietal lobule projections to the presubiculum and neighboring ventromedial temporal cortical areas. *J Comp Neurol* 425, 510-530 (2000).
27. P. S. Goldman-Rakic, L. D. Selemon, M. L. Schwartz, Dual pathways connecting the dorsolateral prefrontal cortex with the hippocampal formation and parahippocampal cortex in the rhesus monkey. *Neuroscience* 12, 719-743 (1984).
28. H. Barbas, G. J. Blatt, Topographically specific hippocampal projections target functionally distinct prefrontal areas in the rhesus monkey. *Hippocampus* 5, 511-533 (1995).
29. J. C. Augustinack, K. Helmer, K. E. Huber, S. Kakunoori, L. Zollei, B. Fischl, Direct visualization of the perforant pathway in the human brain with ex vivo diffusion tensor imaging. *Front Hum Neurosci* 4, 42 (2010).
30. R. Coras, G. Milesi, I. Zucca, A. Mastropietro, A. Scotti, M. Figini, A. Muhlebner, A. Hess, W. Graf, G. Tringali, I. Blumcke, F. Villani, G. Didato, C. Frassoni, R. Spreafico, R. Garbelli, 7T MRI features in control human hippocampus and hippocampal sclerosis: an ex vivo study with histologic correlations. *Epilepsia* 55, 2003-2016 (2014).

31. J. Beaujoin, N. Palomero-Gallagher, F. Boumezbeur, M. Axer, J. Bernard, F. Poupon, D. Schmitz, J. F. Mangin, C. Poupon, Post-mortem inference of the human hippocampal connectivity and microstructure using ultra-high field diffusion MRI at 11.7 T. *Brain Struct Funct* 223, 2157-2179 (2018).
32. R. K. Olsen, J. Robin, Zooming in and zooming out: the importance of precise anatomical characterization and broader network understanding of MRI data in human memory experiments. *Current Opinion in Behavioral Sciences* 32, 57-64 (2020).
33. V. Dinkelacker, R. Valabregue, L. Thivard, S. Lehericy, M. Baulac, S. Samson, S. Dupont, Hippocampal-thalamic wiring in medial temporal lobe epilepsy: Enhanced connectivity per hippocampal voxel. *Epilepsia* 56, 1217-1226 (2015).
34. P. H. Wei, Z. Q. Mao, F. Cong, F. C. Yeh, B. Wang, Z. P. Ling, S. L. Liang, L. Chen, X. G. Yu, In vivo visualization of connections among revised Papez circuit hubs using full q-space diffusion spectrum imaging tractography. *Neuroscience* 357, 400-410 (2017).
35. A. Arrigo, E. Mormina, A. Calamuneri, M. Gaeta, S. Marino, D. Milardi, G. P. Anastasi, A. Quartarone, Amygdalar and hippocampal connections with brainstem and spinal cord: A diffusion MRI study in human brain. *Neuroscience* 343, 346-354 (2017).
36. D. Rangaprakash, G. Deshpande, T. A. Daniel, A. M. Goodman, J. L. Robinson, N. Salibi, J. S. Katz, T. S. Denney, Jr., M. N. Dretsch, Compromised hippocampus-striatum pathway as a potential imaging biomarker of mild-traumatic brain injury and posttraumatic stress disorder. *Hum Brain Mapp* 38, 2843-2864 (2017).
37. B. L. Edlow, J. A. McNab, T. Witzel, H. C. Kinney, The Structural Connectome of the Human Central Homeostatic Network. *Brain Connect* 6, 187-200 (2016).
38. J. J. Maller, T. Welton, M. Middione, F. M. Callaghan, J. V. Rosenfeld, S. M. Grieve, Revealing the Hippocampal Connectome through Super-Resolution 1150-Direction Diffusion MRI. *Sci Rep* 9, 2418 (2019).
39. M. F. Glasser, T. S. Coalson, E. C. Robinson, C. D. Hacker, J. Harwell, E. Yacoub, K. Ugurbil, J. Andersson, C. F. Beckmann, M. Jenkinson, S. M. Smith, D. C. Van Essen, A multi-modal parcellation of human cerebral cortex. *Nature* 536, 171-178 (2016).
40. L. Tang, P. J. Pruitt, Q. Yu, R. Homayouni, A. M. Daugherty, J. S. Damoiseaux, N. Ofen, Differential Functional Connectivity in Anterior and Posterior Hippocampus Supporting the Development of Memory Formation. *Front Hum Neurosci* 14, 204 (2020).
41. J. Poppenk, M. Moscovitch, A hippocampal marker of recollection memory ability among healthy young adults: contributions of posterior and anterior segments. *Neuron* 72, 931-937 (2011).
42. A. Adnan, A. Barnett, M. Moayedi, C. McCormick, M. Cohn, M. P. McAndrews, Distinct hippocampal functional networks revealed by tractography-based parcellation. *Brain Struct Funct* 221, 2999-3012 (2016).
43. A. J. Barnett, W. Reilly, H. R. Dimsdale-Zucker, E. Mizrak, Z. Reagh, C. Ranganath, Intrinsic connectivity reveals functionally distinct cortico-hippocampal networks in the human brain. *PLoS Biol* 19, e3001275 (2021).
44. D. J. Kravitz, K. S. Saleem, C. I. Baker, M. Mishkin, A new neural framework for visuospatial processing. *Nat Rev Neurosci* 12, 217-230 (2011).
45. D. R. Addis, K. Knapp, R. P. Roberts, D. L. Schacter, Routes to the past: neural substrates of direct and generative autobiographical memory retrieval. *NeuroImage* 59, 2908-2922 (2012).
46. P. Zeidman, S. L. Mullally, E. A. Maguire, Constructing, Perceiving, and Maintaining Scenes: Hippocampal Activity and Connectivity. *Cereb Cortex* 25, 3836-3855 (2015).
47. A. C. Lee, K. H. Brodersen, S. R. Rudebeck, Disentangling spatial perception and spatial memory in the hippocampus: a univariate and multivariate pattern analysis fMRI study. *J Cogn Neurosci* 25, 534-546 (2013).
48. P. Zeidman, E. A. Maguire, Anterior hippocampus: the anatomy of perception, imagination and episodic memory. *Nat Rev Neurosci* 17, 173-182 (2016).
49. M. A. Ferguson, C. Lim, D. Cooke, R. R. Darby, O. Wu, N. S. Rost, M. Corbetta, J. Grafman, M. D. Fox, A human memory circuit derived from brain lesions causing amnesia. *Nat Commun* 10, 3497 (2019).
50. M. A. Dalton, E. A. Maguire, The pre/parasubiculum: a hippocampal hub for scene-based cognition? *Curr Opin Behav Sci* 17, 34-40 (2017).

51. R. E. Smith, J. D. Tournier, F. Calamante, A. Connelly, SIFT2: Enabling dense quantitative assessment of brain white matter connectivity using streamlines tractography. *NeuroImage* 119, 338-351 (2015).
52. J. L. Andersson, S. Skare, J. J. N. Ashburner, How to correct susceptibility distortions in spin-echo echo-planar images: application to diffusion tensor imaging. *NeuroImage* 20, 870-888 (2003).
53. P. A. Yushkevich, J. Piven, H. C. Hazlett, R. G. Smith, S. Ho, J. C. Gee, G. Gerig, User-guided 3D active contour segmentation of anatomical structures: Significantly improved efficiency and reliability. *NeuroImage* 31, 1116-1128 (2006).
54. M. A. Dalton, P. Zeidman, D. N. Barry, E. Williams, E. A. Maguire, Segmenting subregions of the human hippocampus on structural magnetic resonance image scans: An illustrated tutorial. *Brain Neurosci Adv* 1, 2398212817701448 (2017).
55. M. J. Valenzuela, F. E. Matthews, C. Brayne, P. Ince, G. Halliday, J. J. Kril, M. A. Dalton, K. Richardson, G. Forster, P. S. Sachdev, F. Medical Research Council Cognitive, S. Ageing, Multiple biological pathways link cognitive lifestyle to protection from dementia. *Biol Psychiatry* 71, 783-791 (2012).
56. P. Zeidman, A. Lutti, E. A. Maguire, Investigating the functions of subregions within anterior hippocampus. *Cortex* 73, 240-256 (2015).
57. J. Kulaga-Yoskovitz, B. C. Bernhardt, S. J. Hong, T. Mansi, K. E. Liang, A. J. van der Kouwe, J. Smallwood, A. Bernasconi, N. Bernasconi, Multi-contrast submillimetric 3 Tesla hippocampal subfield segmentation protocol and dataset. *Sci Data* 2, 150059 (2015).
58. N. Bernasconi, A. Bernasconi, Z. Caramanos, S. B. Antel, F. Andermann, D. L. Arnold, Mesial temporal damage in temporal lobe epilepsy: a volumetric MRI study of the hippocampus, amygdala and parahippocampal region. *Brain* 126, 462-469 (2003).
59. J.-D. Tournier, R. Smith, D. Raffelt, R. Tabbara, T. Dhollander, M. Pietsch, D. Christiaens, B. Jeurissen, C.-H. Yeh, A. Connelly, MRtrix3: A fast, flexible and open software framework for medical image processing and visualisation. *NeuroImage* 202, 116137 (2019).
60. J. D. Tournier, F. Calamante, A. Connelly, MRtrix: Diffusion tractography in crossing fiber regions. *Int J Imag Syst Tech* 22, 53-66 (2012).
61. O. Civier, R. E. Smith, C. H. Yeh, A. Connelly, F. Calamante, Is removal of weak connections necessary for graph-theoretical analysis of dense weighted structural connectomes from diffusion MRI? *NeuroImage* 194, 68-81 (2019).
62. N. J. Tustison, B. B. Avants, P. A. Cook, Y. Zheng, A. Egan, P. A. Yushkevich, J. C. Gee, N4ITK: improved N3 bias correction. *IEEE Trans Med Imaging* 29, 1310-1320 (2010).
63. B. Jeurissen, J.-D. Tournier, T. Dhollander, A. Connelly, J. Sijbers, Multi-tissue constrained spherical deconvolution for improved analysis of multi-shell diffusion MRI data. *NeuroImage* 103, 411-426 (2014).
64. J.-D. Tournier, F. Calamante, D. G. Gadian, A. J. N. Connelly, Direct estimation of the fiber orientation density function from diffusion-weighted MRI data using spherical deconvolution. *NeuroImage* 23, 1176-1185 (2004).
65. J. D. Tournier, F. Calamante, A. Connelly, Robust determination of the fibre orientation distribution in diffusion MRI: non-negativity constrained super-resolved spherical deconvolution. *NeuroImage* 35, 1459-1472 (2007).
66. R. E. Smith, J. D. Tournier, F. Calamante, A. Connelly, Anatomically-constrained tractography: improved diffusion MRI streamlines tractography through effective use of anatomical information. *NeuroImage* 62, 1924-1938 (2012).
67. S. M. Smith, Fast robust automated brain extraction. Human brain mapping 17, 143-155 (2002).
68. Y. Zhang, M. Brady, S. Smith, Segmentation of brain MR images through a hidden Markov random field model and the expectation-maximization algorithm. *IEEE Trans Med Imaging* 20, 45-57 (2001).
69. B. Patenaude, S. M. Smith, D. N. Kennedy, M. Jenkinson, A Bayesian model of shape and appearance for subcortical brain segmentation. *NeuroImage* 56, 907-922 (2011).
70. S. M. Smith, M. Jenkinson, M. W. Woolrich, C. F. Beckmann, T. E. Behrens, H. Johansen-Berg, P. R. Bannister, M. De Luca, I. Drobnjak, D. E. Flitney, R. K. Niazy, J. Saunders, J. Vickers, Y. Zhang, N. De Stefano, J. M. Brady, P. M. Matthews, Advances in functional and structural MR image analysis and implementation as FSL. *NeuroImage* 23 Suppl 1, S208-219 (2004).

71. R. E. Smith, J.-D. Tournier, F. Calamante, A. Connelly, SIFT2: Enabling dense quantitative assessment of brain white matter connectivity using streamlines tractography. *NeuroImage* 119, 338-351 (2015).
72. J. D. Tournier, F. Calamante, A. Connelly, in Proceedings of the international society for magnetic resonance in medicine. (*ISMRM*, 2010), vol. 18, pp. 1670.
73. H. M. Duvernoy, The Human Hippocampus Functional Anatomy, Vascularization and Serial Sections with MRI (Springer-Verlag, Berlin, Heidelberg, 2005).
74. R. E. Smith, J. D. Tournier, F. Calamante, A. Connelly, The effects of SIFT on the reproducibility and biological accuracy of the structural connectome. *NeuroImage* 104, 253-265 (2015).
75. B. Fischl, FreeSurfer. *NeuroImage* 62, 774-781 (2012).
76. M. Tahedl, B.A.T.M.A.N: Basic and Advanced Tractography with MRtrix for All Neurophiles. https://doi.org/10.17605/OSF.IO/FKYHT, (2020, May 25).
77. F. Calamante, J. D. Tournier, R. E. Smith, A. Connelly, A generalised framework for super-resolution track-weighted imaging. *NeuroImage* 59, 2494-2503 (2012).
78. F. Calamante, J. D. Tournier, G. D. Jackson, A. Connelly, Track-density imaging (TDI): Super-resolution white matter imaging using whole-brain track-density mapping. *NeuroImage* 53, 1233-1243 (2010).
79. B. B. Avants, P. Yushkevich, J. Pluta, D. Minkoff, M. Korczykowski, J. Detre, J. C. Gee, The optimal template effect in hippocampus studies of diseased populations. *NeuroImage* 49, 2457-2466 (2010).
80. K. Amunts, C. Lepage, L. Borgeat, H. Mohlberg, T. Dickscheid, M. E. Rousseau, S. Bludau, P. L. Bazin, L. B. Lewis, A. M. Oros-Peusquens, N. J. Shah, T. Lippert, K. Zilles, A. C. Evans, BigBrain: an ultrahigh-resolution 3D human brain model. *Science* 340, 1472-1475 (2013).

Figures and Tables

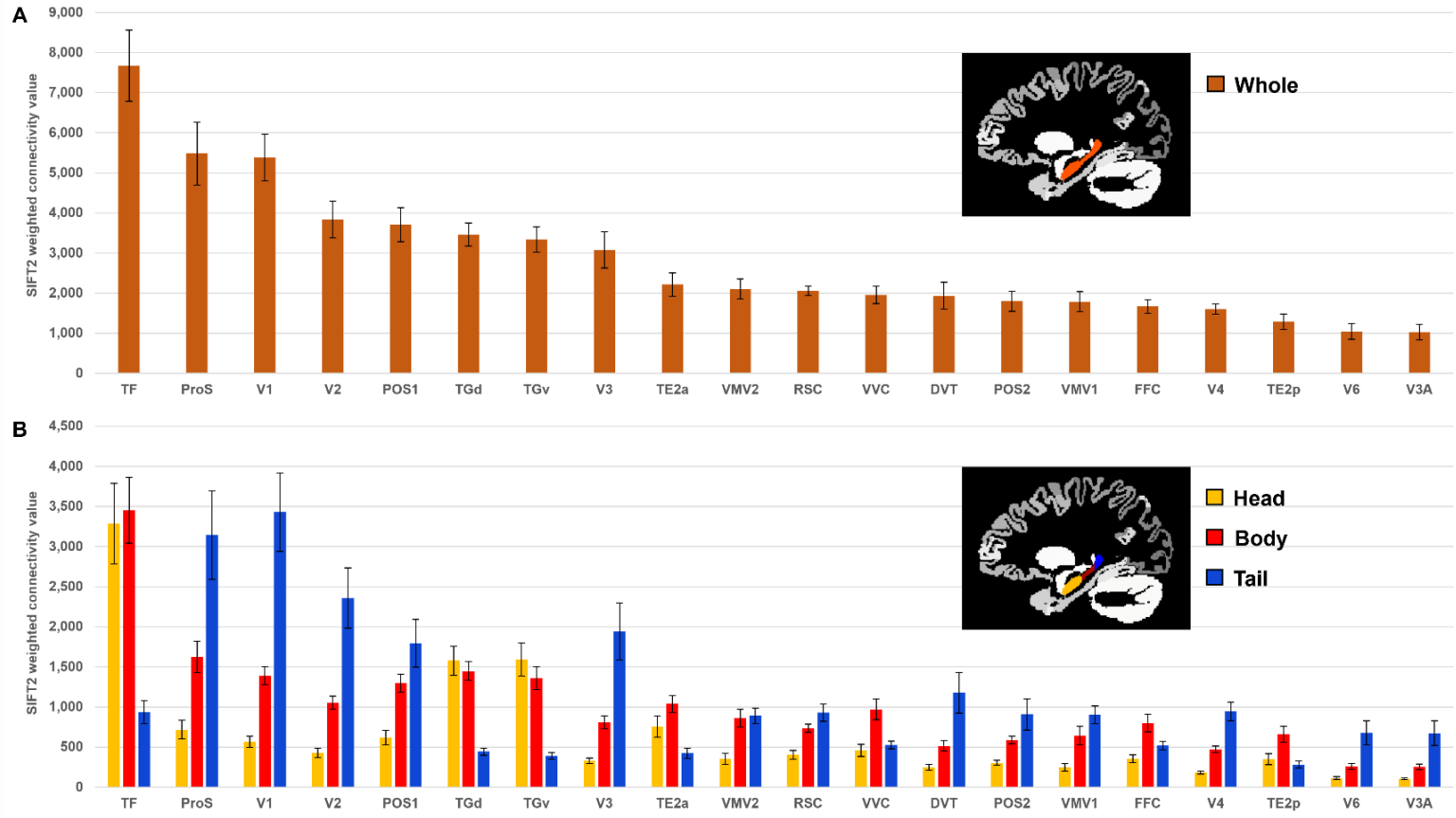

Figure 1. Twenty cortical brain areas with the highest degree of anatomical connectivity with the hippocampus. a. Histogram plotting the mean structural connectivity (given by the sum of SIFT2 weighted values) associated with the twenty cortical areas most strongly connected with the whole hippocampus (excluding medial temporal lobe (MTL) areas; see Supplementary Figure S1 for MTL values). Error bars represent the standard error of the mean. b. Histogram plotting the corresponding mean SIFT2 weighted values associated with anterior (yellow), body (red) and tail (blue) portions of the hippocampus for the twenty most strongly connected cortical areas presented in a. Errors bars represent the standard error of the mean.

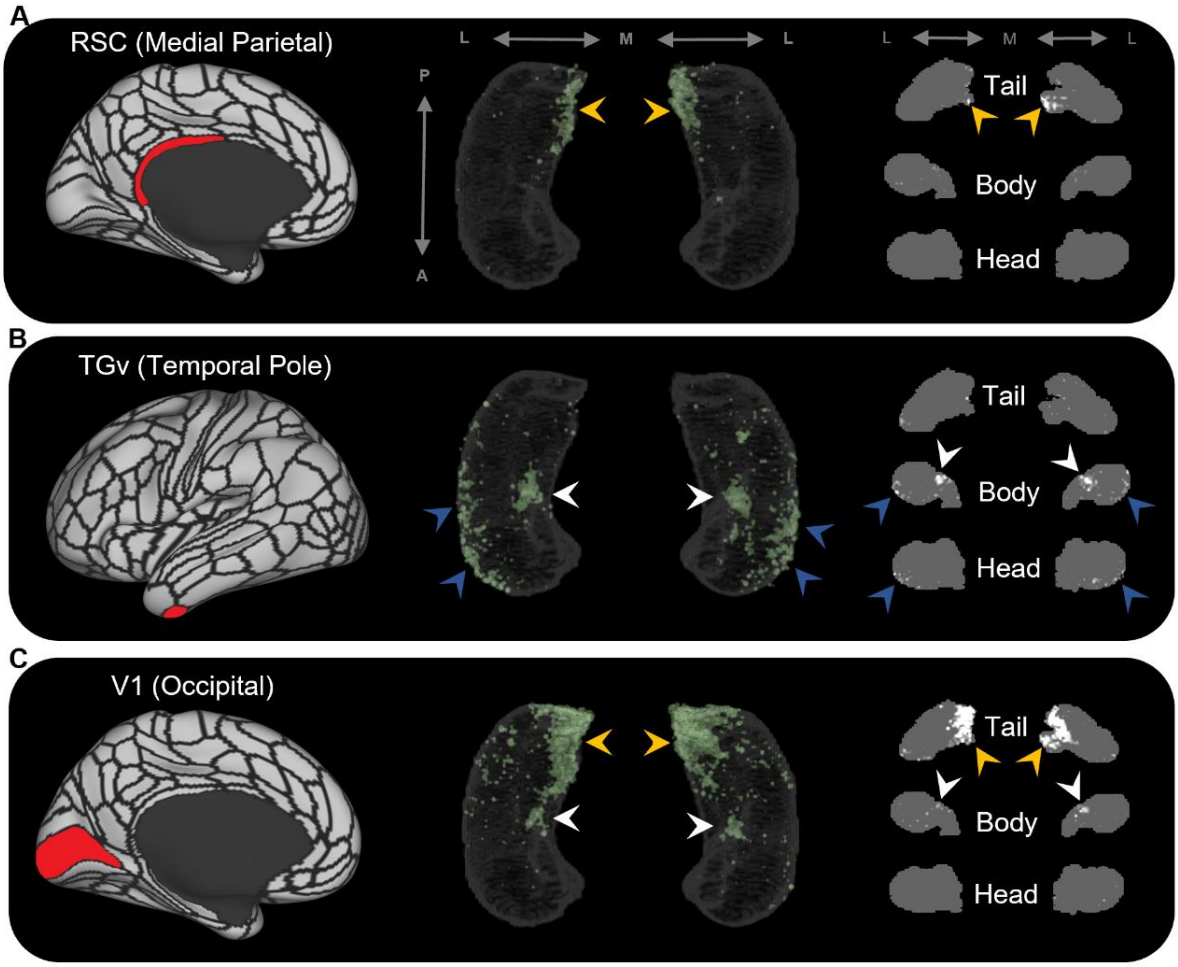

Figure 2. Representative examples of the spatial distribution of endpoint density within the hippocampus for different cortical brain areas. Representative examples of the location of endpoint densities associated with RSC in the medial parietal lobe (a), TGv in the temporal pole (b) and V1 in the occipital lobe (c). In each panel, the location of the relevant brain area is indicated in red on the brain map (left); a 3D rendered representation of the bilateral group level hippocampus mask is presented (middle; transparent grey) overlaid with the endpoint density map associated with each brain area (green); representative slices of the head, body and tail of the hippocampus are displayed in the coronal plane (right; grey) and overlaid with endpoint density maps (white). Note, the spatial distribution of endpoint density within the hippocampus associated with each brain area differs along both the anterior-posterior and medial-lateral axes of the hippocampus. RSC and V1 displayed greatest endpoint density in the posterior medial hippocampus (yellow arrows in a and c). In contrast, TGv displayed greatest endpoint density in the anterior lateral hippocampus and in a circumscribed region in the anterior medial hippocampus (blue and white arrows respectively in b). Area V1 also expressed endpoint density in a circumscribed region in the anterior medial hippocampus (white arrows in c). A=anterior; P=posterior; M=medial; L=lateral.

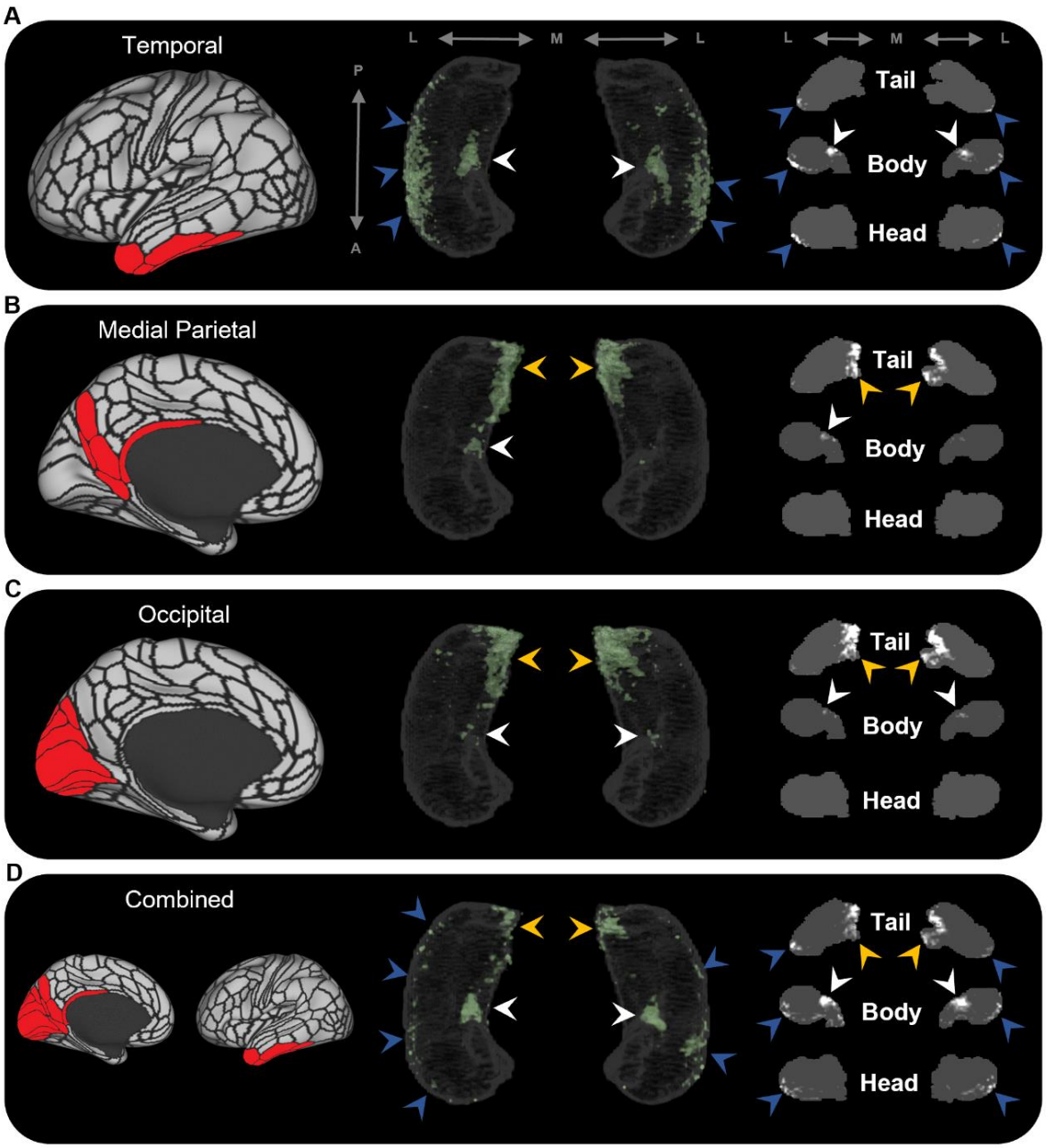

Figure 3. Averaged endpoint density maps for anatomically related brain areas. We averaged the endpoint density maps for the mostly highly connected brain areas in temporal (a; TF, TGd, TGv, TE2a, TE2p), medial parietal (b; ProS, POS1, RSC, DVT, POS2) and occipital (c; V1-4, V6, V3a) cortices and each of these regions combined (d). In each panel, the location of the relevant brain areas are indicated in red on the brain map (left); a 3D rendered representation of the bilateral group level hippocampus mask is presented (middle; transparent grey) overlaid with the endpoint density map associated with each collection of brain areas; representative slices of the head, body and tail of the hippocampus are displayed in the coronal plane (right; grey) and overlaid with endpoint density maps (white). Average endpoint density associated with temporal areas (a) was primarily localised along the anterior lateral hippocampus and a circumscribed region in the anterior medial hippocampus (blue and white arrows respectively). Average endpoint density associated with medial parietal (b) and occipital (c) areas was primarily localised to the posterior medial hippocampus (yellow arrows) and, to a lesser degree, circumscribed regions in the anterior medial hippocampus (white arrows). Average endpoint density associated with these temporal, medial parietal and occipital brain areas combined (d) was localised to circumscribed regions in the posterior and anterior medial hippocampus (yellow and white arrows

respectively) and in punctate clusters along the anterior-posterior extent of the lateral hippocampus (blue arrows) suggesting that these specific regions within the hippocampus are highly connected with multiple cortical areas. A=anterior; P=posterior; M=medial; L=lateral.

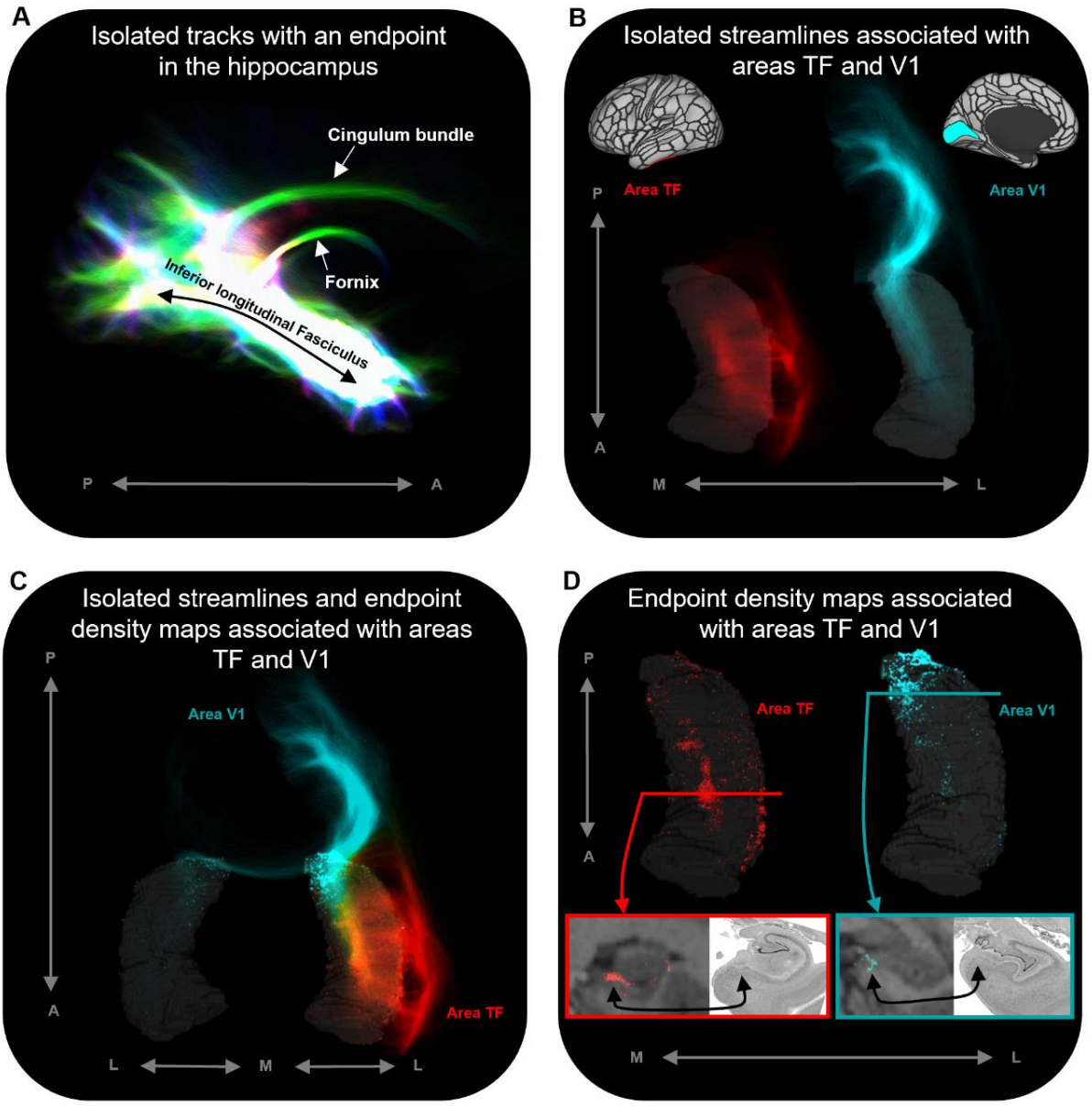

Figure 4. Representative examples of single subject analysis. a. 3D rendering of the hippocampus tractogram for a single participant showing isolated tracks with an endpoint in the hippocampus viewed in the sagittal plane (displayed with transparency; high intensity represents high density of tracks). b. 3D rendered left hippocampus masks (transparent grey) for the same participant overlaid with isolated streamlines associated with the left hemisphere areas TF (red) and V1 (turquoise). The location of areas TF and V1 are indicated on the brain maps (top). c. 3D rendered bilateral hippocampus mask for the same participant (transparent grey) overlaid with isolated streamlines and endpoint density maps associated with the left hemisphere areas TF (red) and V1 (turquoise). Note, while streamlines associated with areas TF and V1 are primarily ipsilateral in nature, streamlines associated with V1 also project to the contralateral hippocampus. d. 3D rendered left hippocampus masks (transparent grey) for the same participant overlaid with endpoint density maps associated with areas TF (red) and V1 (turquoise). For TF and V1, we present a coronal section of the T1-weighted structural image overlaid with the endpoint density maps and a corresponding slice of post-mortem hippocampal tissue (from a different subject) for anatomical comparison (bottom). For both TF (red border; level of the uncal apex) and V1 (turquoise border; level of the hippocampal tail), endpoint density is primarily localised to a circumscribed region in the medial hippocampus aligning with the location of the distal

subiculum/proximal presubiculum (black arrows; also see Figure 5a). Post-mortem images are from the BigBrain Project (80). A=anterior; P=posterior; M=medial; L=lateral.

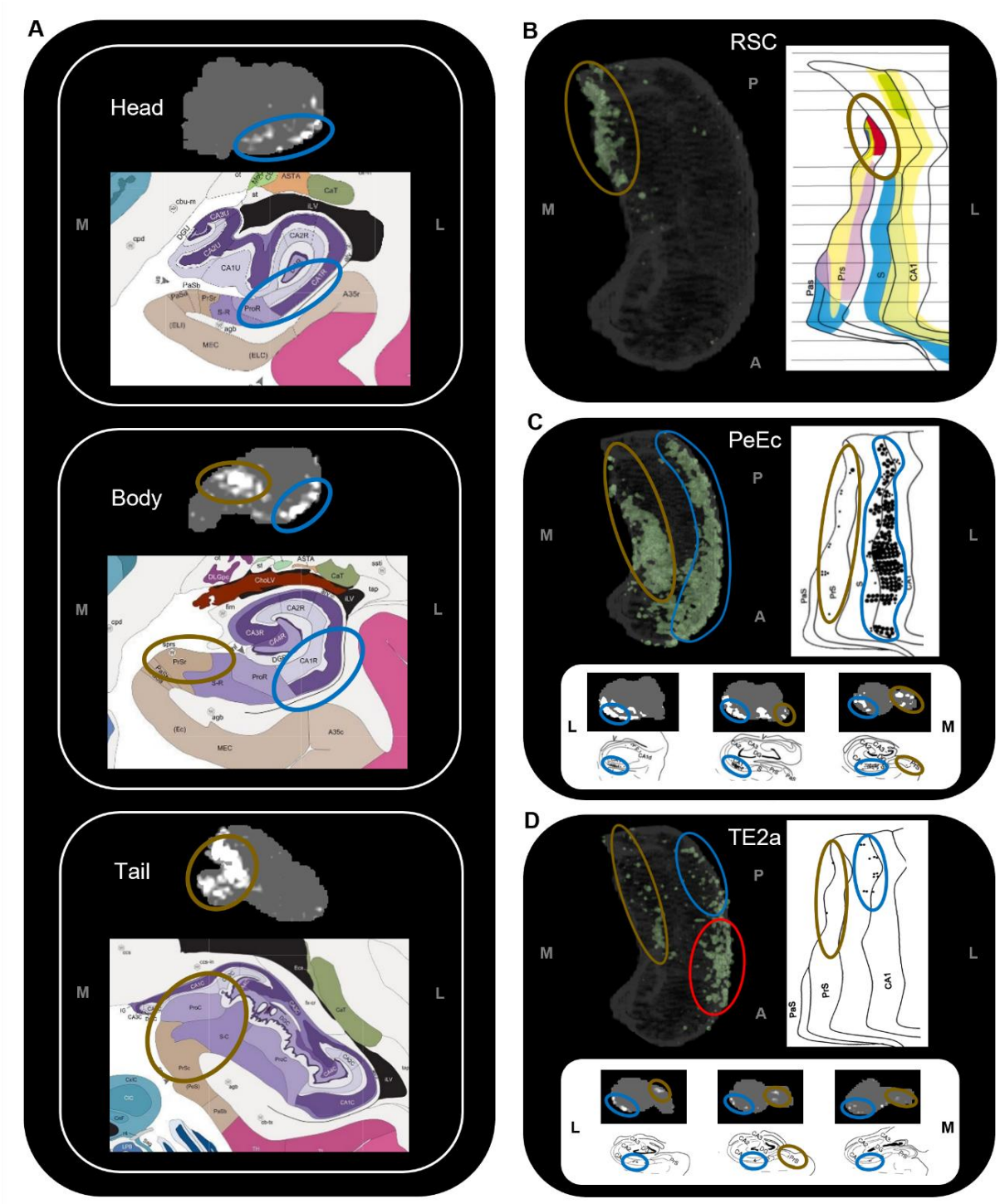

Figure 5. Anatomical location of endpoint densities within the hippocampus and comparison with results of non-human primate studies. a. Representative slices of the head (top), body (middle) and tail (bottom) of the hippocampus displayed in the coronal plane (grey) and overlaid with group level endpoint density maps associated with area TF (head and body; white) and V1 (tail; white). Schematic representations of roughly equivalent slices of the hippocampus showing hippocampal subfields are displayed below each slice (from the Allen Adult Human Brain Atlas website: https://atlas.brain-map.org/). Note, endpoint density in the lateral hippocampus (blue ellipsoids) aligns with the location of the distal CA1/proximal subiculum. Endpoint density in the medial hippocampus (brown ellipsoids) aligns with the location of distal subiculum/proximal presubiculum. b-d. 3D rendered representations of the group level hippocampus mask (left; transparent grey) are overlaid with endpoint density maps

(green) associated with RSC (b), PeEc (c) and TE2a (d). Schematic representations of the macaque hippocampus (right; Images reproduced with permission from (22)) show the location of labelled cells following retrograde tracer injection into the RSC (b; red), PeEc (c; black points) and TE2a (d; black points). The bottom panel of c and d displays slices of human hippocampus in the coronal plane (grey) overlaid with endpoint density maps (white) and roughly equivalent slices of the macaque hippocampus display the location of labelled cells (black points; Images reproduced with permission from (22)). Note, endpoint density and labelled cells in the human and macaque respectively are localised to similar regions along the anterior-posterior, lateral (blue ellipsoids) and medial (brown ellipsoids) hippocampus. However, areas of difference also exist (d; red ellipsoid). M=medial; L=lateral; A=anterior; P=posterior.

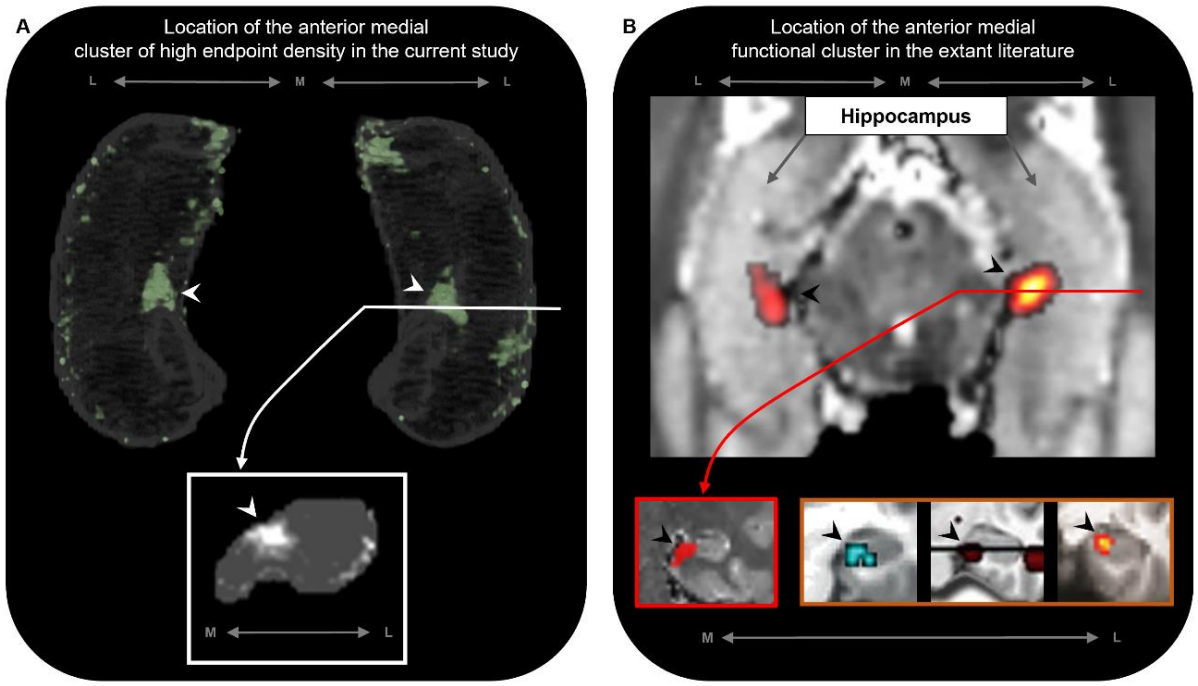

Figure 6. The location of the anterior medial anatomical cluster aligns with the location of a commonly observed anterior medial functional cluster. a. A 3D rendered representation of the bilateral group level hippocampus mask (top; transparent grey) is presented overlaid with the endpoint density map averaged across the most highly connected brain areas in temporal, medial parietal and occipital cortices (green; see Figure 3d for details); a representative slice of hippocampus in the coronal plane (bottom panel; grey) at the level of the uncal apex (indicated by white line) is presented overlaid with the endpoint density map (white). b. An axial section of a T2-weighted image (top; from a separate study) showing the bilateral hippocampus overlaid with the location of a circumscribed functional cluster observed in the anterior medial hippocampus during a functional MRI investigation of visuospatial mental imagery (5). A representative slice of the hippocampus (bottom left panel; red border) at the level of the uncal apex (indicated by red line) is presented to show the location of this anterior medial functional cluster in the coronal plane (images reproduced with permission from (5)). Circumscribed functional clusters in the anterior medial hippocampus are commonly observed in studies of 'scene-based visuospatial cognition' such as episodic memory and prospection (bottom right panel; orange border). Images reproduced with permission from (46) (left), (45) (middle) and (47) (right). Note, the location of these commonly observed functional clusters in the anterior medial hippocampus (black arrows in panel b) align with the location of the anatomical cluster in the anterior medial hippocampus observed in the current study (white arrows in panel a). M=medial; L=lateral.

Table 1. Twenty cortical brain areas (excluding medial temporal lobe) with the highest degree of anatomical connectivity with the whole hippocampus. Column 1 displays cortical areas as defined by the Human Connectome Project Multi-Modal Parcellation (HCPMMP) scheme and ordered by strength of connectivity with the whole hippocampus (abbreviations for all cortical areas are defined in Supplementary Table S3). Column 2 indicates the broader brain region within which each cortical area is located. Column 3 displays the mean SIFT2 weighted value (connectivity strength) associated with each brain area. Column 4 displays the standard error of the mean. Column 5 displays the percent of all cortical connections accounted for by each area. Values in brackets indicate the percent of cortical connections accounted for by each area when excluding medial temporal lobe (MTL) areas.

Cortical area	Location of area	Whole hippocampus		
		Mean SIFT2 weighted value (connectivity strength; n=10)	SE of mean	Percent of all cortical connections accounted for by area. (Percent of cortical connections excluding MTL areas)
TF	Lateral Temporal Cortex	7673	886	5.10 (10.61)
ProS	Medial Parietal Cortex (including Posterior Cingulate)	5483	784	3.64 (7.58)
V1	Early Visual Cortex (Occipital)	5385	579	3.58 (7.45)
V2	Early Visual Cortex (Occipital)	3840	462	2.55 (5.31)
POS1	Medial Parietal Cortex (including Posterior Cingulate)	3712	424	2.47 (5.13)
TGd	Temporal Pole	3465	288	2.30 (4.79)
TGv	Temporal Pole	3337	313	2.22 (4.61)
V3	Early Visual Cortex (Occipital)	3079	450	2.05 (4.26)
TE2a	Lateral Temporal Cortex	2214	288	1.47 (3.06)
VMV2	Ventral Stream Visual Cortex	2105	247	1.40 (2.91)
RSC	Medial Parietal Cortex (including Posterior Cingulate)	2063	121	1.37 (2.85)
VVC	Ventral Stream Visual Cortex	1956	220	1.30 (2.71)
DVT	Medial Parietal Cortex (including Posterior Cingulate)	1939	335	1.29 (2.68)
POS2	Medial Parietal Cortex (including Posterior Cingulate)	1802	248	1.20 (2.49)
VMV1	Ventral Stream Visual Cortex	1788	248	1.19 (2.47)
FFC	Ventral Stream Visual Cortex	1670	172	1.11 (2.31)
V4	Early Visual Cortex (Occipital)	1601	127	1.06 (2.21)

TE2p	Lateral Temporal Cortex	1288	198	0.86 (1.78)
V6	Dorsal Stream Visual Cortex	1050	195	0.70 (1.45)
V3A	Dorsal Stream Visual Cortex	1029	197	0.68 (1.42)

Table 2. Connectivity between the twenty most highly connected cortical areas and the head, body and tail of the hippocampus. Column 1 displays cortical areas as defined by the Human Connectome Project Multi-Modal Parcellation (HCPMMP) scheme and ordered by strength of connectivity with the whole hippocampus (abbreviations for all cortical areas are defined in Supplementary Table S3). Column 2 designates the portion of hippocampus (head, body, tail). Column 3 displays the mean SIFT2 weighted value (connectivity strength) between each cortical area and the head, body and tail of the hippocampus. Column 4 displays the standard error of the mean. Column 5 displays the contrast for each paired samples t-test. Column 6 displays the t-statistic associated with each pair. Column 7 displays the p-value associated with each pair. Column 8 indicates the significance level associated with each pair following Bonferroni correction. *** = <0.001, ** = <0.01, * = <0.05, n.s. = not statistically significant.

Cortical area	**Portion of hippocampus**	**Mean SIFT2 weighted value (connectivity strength; n=10)**	**SE of Mean**	**Paired samples t-test**			
				Pair	***t*-statistic *t*(9)**	***p*-value**	**Significance**
TF	Head	3287	500	Head - body	-0.34	0.741	n.s.
	Body	3452	410	Body - tail	9.077	<0.001	***
	Tail	934	144	Head - tail	5.049	0.001	**
ProS	Head	716	116	Head - body	-5.75	<0.001	***
	Body	1625	194	Body - tail	-3.618	0.006	**
	Tail	3143	553	Head - tail	-4.799	0.001	**
V1	Head	567	70	Head - body	-9.508	<0.001	***
	Body	1389	112	Body - tail	-4.629	0.001	**
	Tail	3429	489	Head - tail	-5.919	<0.001	***
V2	Head	428	62	Head - body	-11.910	<0.001	***
	Body	1054	82	Body - tail	-3.903	0.004	**
	Tail	2358	376	Head - tail	-5.396	<0.001	***
POS1	Head	620	89	Head - body	-6.255	<0.001	***
	Body	1299	112	Body - tail	-2.196	0.056	n.s.
	Tail	1793	297	Head - tail	-4.043	0.003	**
TGd	Head	1576	182	Head - body	0.79	0.450	n.s.
	Body	1446	117	Body - tail	11.378	<0.001	***

	Tail	443	47	Head - tail	6.641	<0.001	***
TGv	Head	1589	207	Head - body	1.121	0.291	n.s.
	Body	1358	144	Body - tail	8.211	<0.001	***
	Tail	389	41	Head - tail	5.973	<0.001	***
V3	Head	327	37	Head - body	-7.204	<0.001	***
	Body	810	83	Body - tail	-3.921	0.004	**
	Tail	1942	357	Head - tail	-4.718	0.001	**
TE2a	Head	754	132	Head - body	-3.759	0.004	**
	Body	1038	107	Body - tail	11.479	<0.001	***
	Tail	422	65	Head - tail	3.787	0.004	**
VMV2	Head	354	68	Head - body	-7.919	<0.001	***
	Body	860	111	Body - tail	-0.375	0.716	n.s.
	Tail	891	97	Head - tail	-6.248	<0.001	***
RSC	Head	401	55	Head - body	-8.647	<0.001	***
	Body	733	52	Body - tail	-1.55	0.155	n.s.
	Tail	928	107	Head - tail	-3.727	0.005	**
VVC	Head	460	76	Head - body	-5.554	<0.001	***
	Body	969	129	Body - tail	4.058	0.003	**
	Tail	528	48	Head - tail	-0.885	0.399	n.s.
DVT	Head	247	36	Head - body	-5.436	<0.001	***
	Body	515	65	Body - tail	-3.374	0.008	**
	Tail	1178	253	Head - tail	-3.954	0.003	**
POS2	Head	303	32	Head - body	-6.682	<0.001	***
	Body	590	47	Body - tail	-2.02	0.074	n.s.
	Tail	909	195	Head - tail	-3.211	0.011	*
VMV1	Head	245	47	Head - body	-5.392	<0.001	***
	Body	644	115	Body - tail	-2.939	0.017	n.s. (following Bonferroni correction)

	Tail	899	110	Head - tail	-7.372	<0.001	***
FFC	Head	355	49	Head - body	-5.364	<0.001	***
	Body	798	109	Body - tail	2.805	0.021	n.s. (following Bonferroni correction)
	Tail	517	55	Head - tail	-2.24	0.052	n.s.
V4	Head	183	20	Head - body	-10.472	<0.001	***
	Body	472	40	Body - tail	-4.002	0.003	**
	Tail	946	116	Head - tail	-6.136	<0.001	***
TE2p	Head	348	69	Head - body	-5.453	<0.001	***
	Body	658	101	Body - tail	5.168	0.001	**
	Tail	282	45	Head - tail	1.163	0.275	n.s.
V6	Head	113	16	Head - body	-5.428	<0.001	***
	Body	259	37	Body - tail	-3.652	0.005	**
	Tail	678	149	Head - tail	-4.047	0.003	**
V3A	Head	103	11	Head - body	-5.641	<0.001	***
	Body	252	35	Body - tail	-3.46	0.007	**
	Tail	674	155	Head - tail	-3.895	0.004	**

Supplementary Information

Note S1: Additional medial temporal lobe analyses.

While the primary focus of our study was to characterise anatomical connectivity between the hippocampus and non-medial temporal lobe (MTL) cortical areas, we also characterised patterns of connectivity between the hippocampus and MTL cortical areas. Cortical areas within the MTL were highly connected with the hippocampus and cumulatively accounted for 52% of all cortical connections. The most highly connected area was the EC (24% of all cortical connections) followed by PeEc (14%), PHA2 (6%), PHA1 (5%) and PHA3 (3%) (see Figure S1a and Table S1). Results of the anterior-posterior axis analyses revealed that the EC and PeEc displayed a gradient style anterior-to-posterior decrease in connectivity. In contrast, PHA1-3 each displayed the highest degree of connectivity with the body of the hippocampus and lower connectivity with both the head and tail of the hippocampus (Figure S1b and Table S2).

The results of the group level endpoint analyses showed that MTL cortical areas had dense patterns of connectivity with the hippocampus. For example, the EC displayed high endpoint density along the entire anterior-posterior axis of the hippocampus. Although difficult to visualise due to the high density of endpoints, the results of our anterior-posterior analysis showed that endpoint density was greatest in the head and body of the hippocampus (see Figure S1b and Table S2). Endpoint density was primarily located in portions of the hippocampus aligning with the location of the CA1, subiculum, pre- and parasubiculum (See Figure S2a).

Endpoint density expression associated with PeEc differed along the anterior-posterior axis of the hippocampus. In the hippocampal head, endpoint density was more pronounced in the lateral hippocampus primarily aligning with the location of the CA1 and subiculum (indicated by blue arrows in Figure S2b). Moving into the body, expression in the CA1 and subiculum was maintained (indicated by blue arrows in Figure S2b) and additional clusters of endpoint density were expressed in the medial hippocampus aligning with the location of the distal subiculum/proximal presubiculum (indicated by white arrows in Figure S2b). Moving into the hippocampal tail, clusters of endpoint density appeared to be more localised to a lateral region of the hippocampus aligning with the location of distal CA1/proximal subiculum (indicated by blue arrows in Figure S2a) with comparatively weaker expression in medial portions of the hippocampal tail.

Endpoint density associated with PHA1-3 was most pronounced in the body of the hippocampus and primarily localised to lateral areas aligning with the location of CA1 and subiculum (indicated by blue arrows in Figure S2c-e) and in the medial hippocampus aligning with the location of the distal subiculum/proximal presubiculum (indicated by white arrows in Figure S2c-e). PHA1-3 expressed less endpoint density in the hippocampal head which was localised to the lateral hippocampus aligning with the location of CA1 and subiculum (indicated by blue arrows in Figure S2c-e). Moving into the hippocampal tail, clusters of endpoint density were more localised to a lateral region aligning with the location of distal CA1/proximal subiculum (indicated by blue arrows in Figure S2c-e). However, PHA1-3 showed different patterns of endpoint density in the medial aspect of the hippocampal tail. PHA1 and, to a lesser extent, PHA2 displayed endpoint density in the posterior medial hippocampus aligning with the location of the distal subiculum/proximal presubiculum (indicated by yellow arrows in Figure S2c and d). In contrast, PHA3 displayed modest endpoint density in the posterior medial hippocampus.

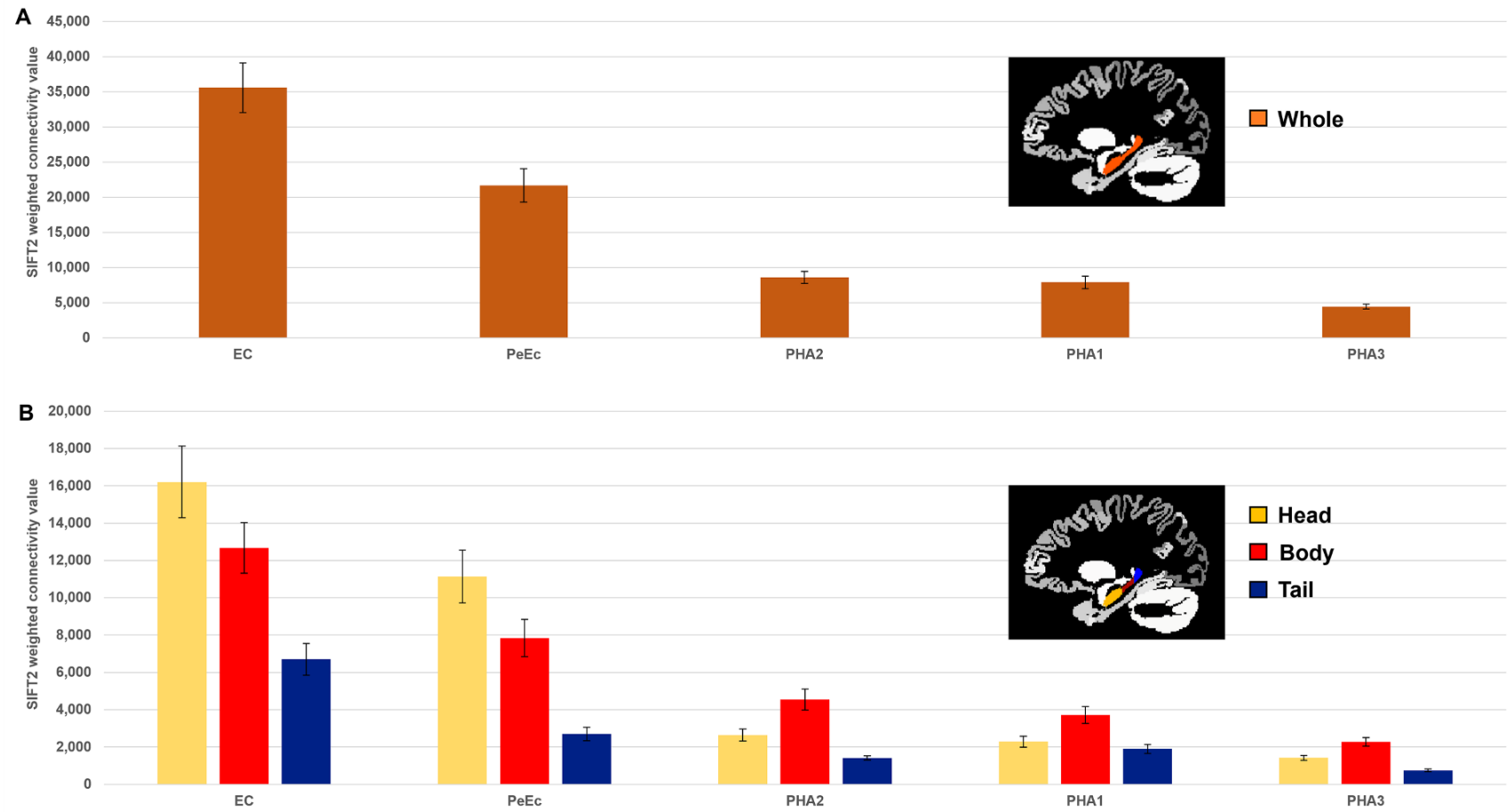

Fig. S1. MTL cortices anatomical connectivity with the hippocampus. a. Histogram plotting the mean structural connectivity (given by the sum of SIFT2 weighted values) associated with MTL cortical areas connected with the whole hippocampus. Error bars represent the standard error of the mean. b. Histogram plotting the corresponding mean SIFT2 weighted values associated with anterior (yellow), body (red) and tail (blue) portions of the hippocampus for MTL cortical areas presented in a. Errors bars represent the standard error of the mean.

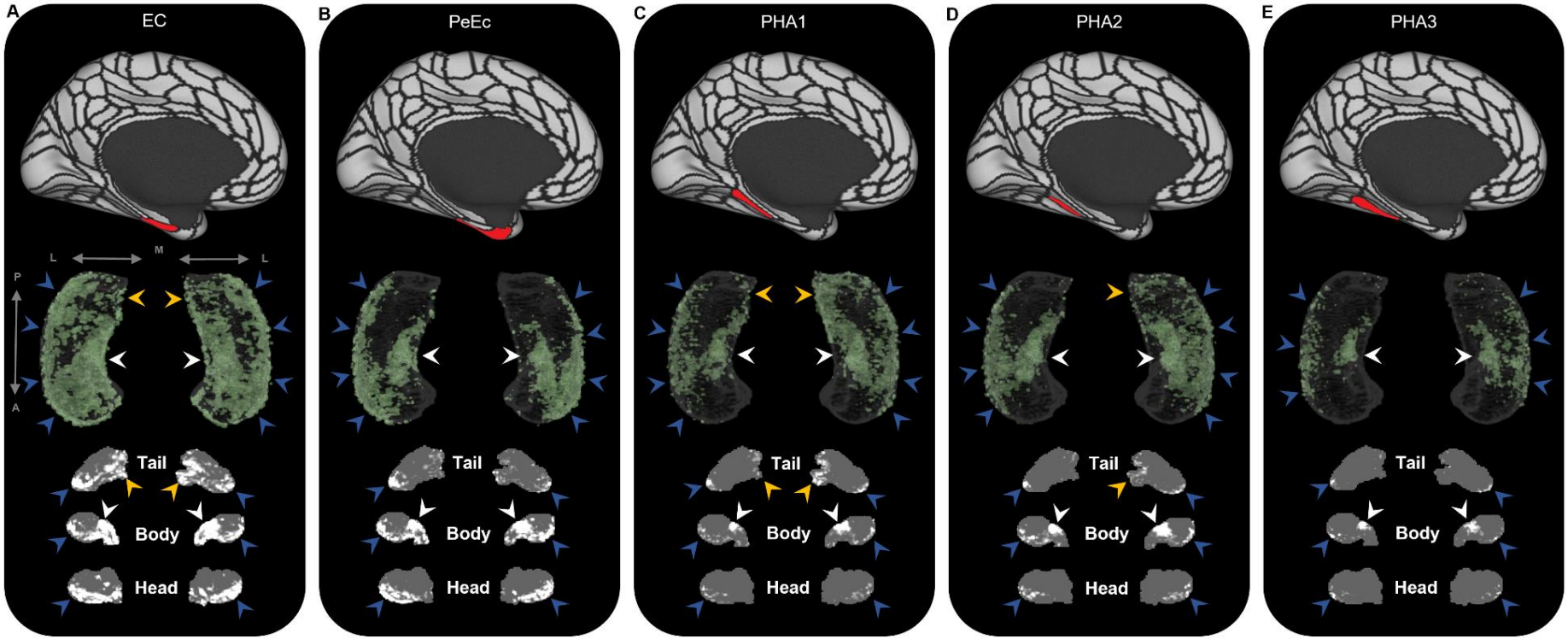

Fig. S2. Representative examples of the spatial distribution of endpoint density within the hippocampus for MTL brain areas. Representative examples of the location of endpoint densities associated with EC (a), PeEc (b) PHA1 (c), PHA2 (d) and PHA3 (e). In each panel, the location of the relevant brain area is indicated in red on the brain map (top); a 3D rendered representation of the bilateral group level hippocampus mask (middle; transparent grey) is presented overlaid with the endpoint density map associated with each brain area (green); representative slices of the head, body and tail of the hippocampus are displayed in the coronal plane (bottom; grey) and overlaid with endpoint density maps (white). Note, as expected, the spatial distribution of endpoint density associated with MTL cortical areas is denser than that observed for non-MTL cortical areas (compare with Figures S3-5). EC displayed high endpoint density throughout the hippocampus (a). PeEc (b) and PHA3 (e) displayed the greatest endpoint density along the anterior-posterior extent of the lateral hippocampus (blue arrows) and in a circumscribed region in the anterior medial hippocampus (white arrows). PeEc and PHA3 showed little endpoint density in the posterior medial hippocampus. PHA1 (c) and PHA2 (d) displayed high endpoint density along the anterior-posterior extent of the lateral hippocampus (blue arrows), in the anterior medial hippocampus (white arrows) and, in contrast to PeEc and PHA3, in the posterior medial hippocampus (yellow arrows). A=anterior; P=posterior; M=medial; L=lateral.

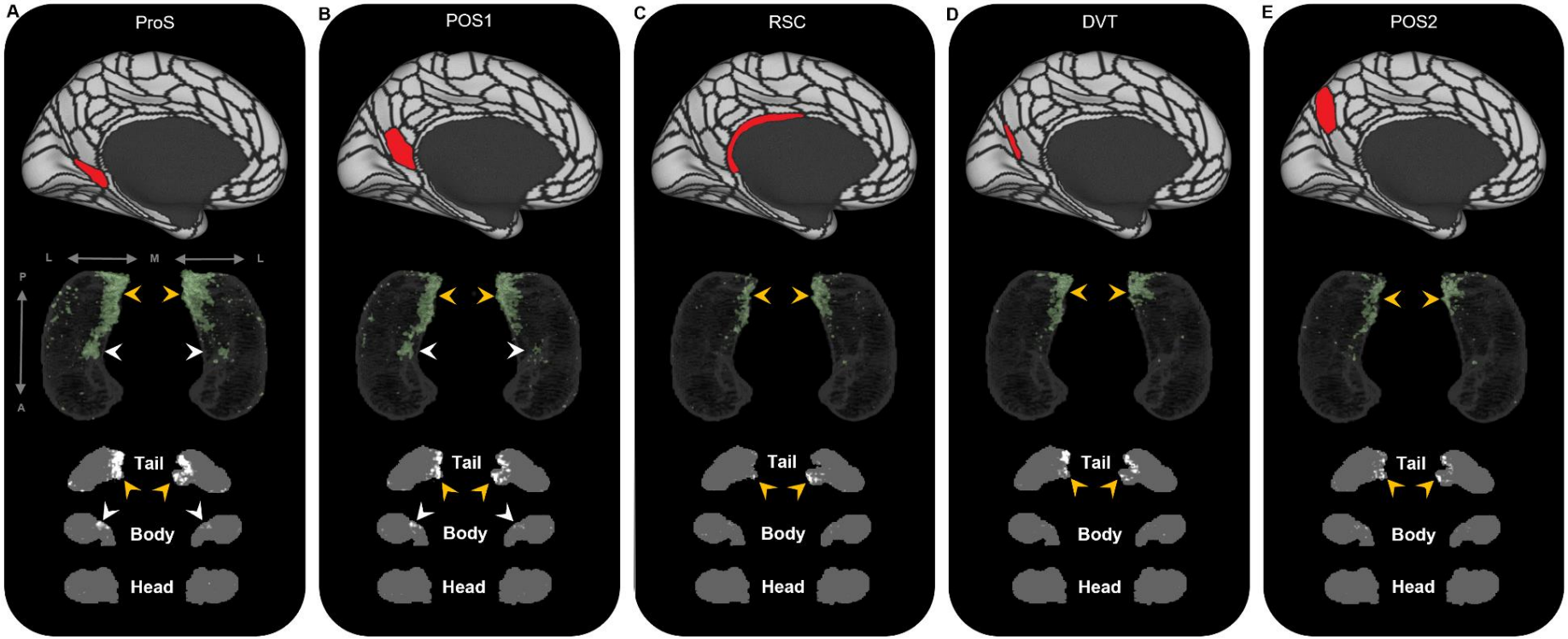

Fig. S3. Representative examples of the spatial distribution of endpoint density within the hippocampus associated with the five most highly connected medial parietal brain areas. Representative examples of the location of endpoint densities associated with ProS (a), POS1 (b) RSC (c), DVT (d) and POS2 (e). In each panel, the location of the relevant brain area is indicated in red on the brain map (top); a 3D rendered representation of the bilateral group level hippocampus mask (middle; transparent grey) is presented overlaid with the endpoint density map associated with each brain area (green); representative slices of the head, body and tail of the hippocampus are displayed in the coronal plane (bottom; grey) and overlaid with endpoint density maps (white). Note, the spatial distribution of endpoint density within the hippocampus associated with each of these medial parietal brain areas is primarily localised to the posterior medial hippocampus (yellow arrows in panels a-e). ProS and POS1 also display clusters of endpoint density in a circumscribed region in the anterior medial hippocampus (white arrows in panels a and b). A=anterior; P=posterior; M=medial; L=lateral.

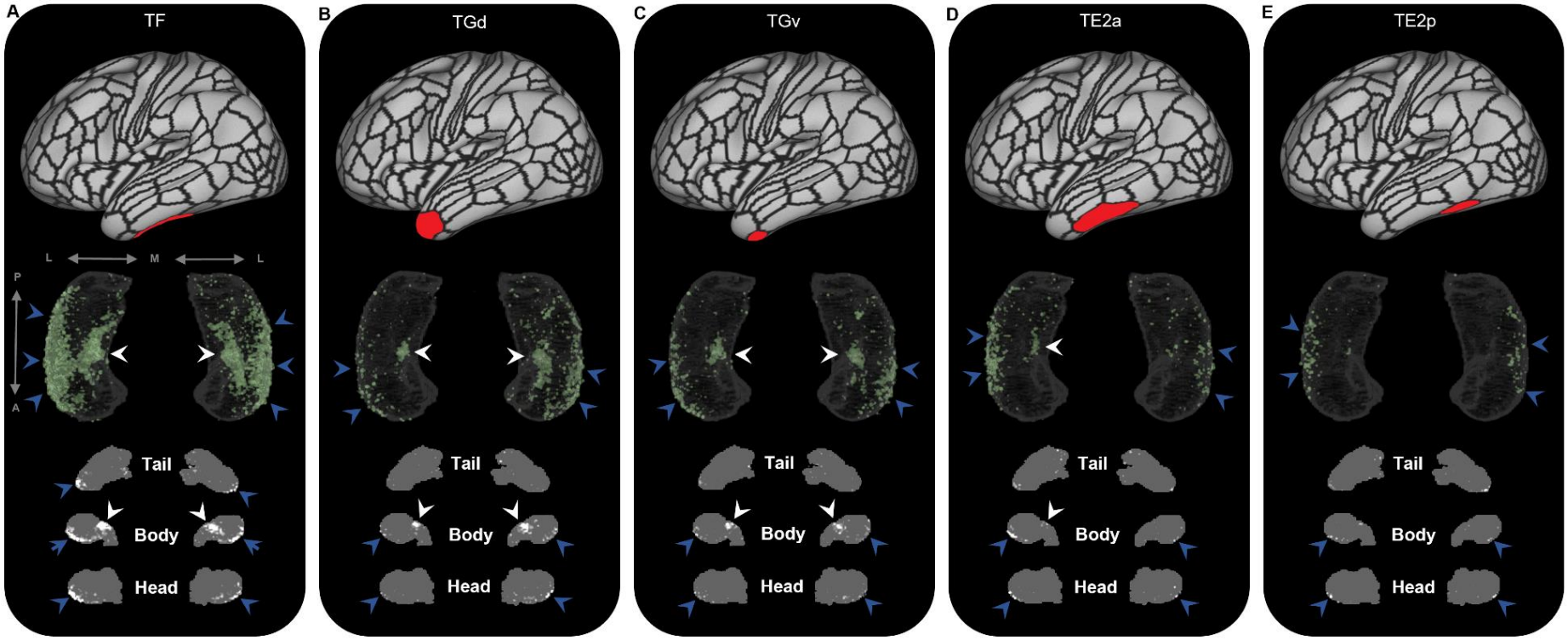

Fig. S4. Representative examples of the spatial distribution of endpoint density within the hippocampus associated with the five most highly connected non-MTL temporal brain areas. Representative examples of the location of endpoint densities associated with TF (a), TGd (b) TGv (c), TE2a (d) and TE2p (e). In each panel, the location of the relevant brain area is indicated in red on the brain map (top); a 3D rendered representation of the bilateral group level hippocampus mask (middle; transparent grey) is presented overlaid with the endpoint density map associated with each brain area (green); representative slices of the head, body and tail of the hippocampus are displayed in the coronal plane (bottom; grey) and overlaid with endpoint density maps (white). Note, the spatial distribution of endpoint density within the hippocampus associated with each of these temporal brain areas is primarily localised to portions of the lateral hippocampal head and body (blue arrows in panels a-e) and a circumscribed region in the anterior medial hippocampus (white arrows in panels a-d). A=anterior; P=posterior; M=medial; L=lateral.

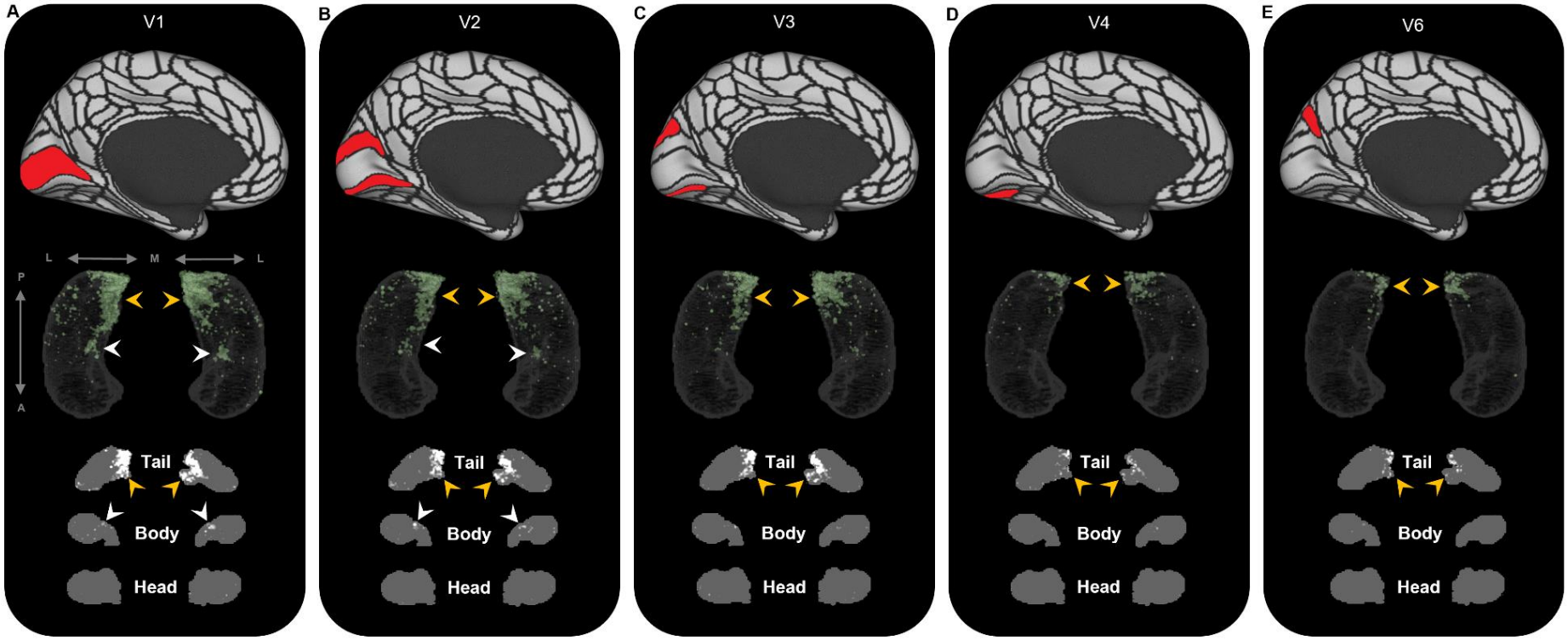

Fig. S5. Representative examples of the spatial distribution of endpoint density within the hippocampus associated with the five most highly connected occipital brain areas. Representative examples of the location of endpoint densities associated with V1 (a), V2 (b) V3 (c), V4 (d) and V6 (e). In each panel, the location of the relevant brain area is indicated in red on the brain map (top); a 3D rendered representation of the bilateral group level hippocampus mask (middle; transparent grey) is presented overlaid with the endpoint density map associated with each brain area (green); representative slices of the head, body and tail of the hippocampus are displayed in the coronal plane (bottom; grey) and overlaid with endpoint density maps (white). Note, the spatial distribution of endpoint density within the hippocampus associated with each of these occipital brain areas is primarily localised to the posterior medial hippocampus (yellow arrows in panels a-f). V1 and V2 also display clusters of endpoint density in a circumscribed region in the anterior medial hippocampus (white arrows in panels a and b). A=anterior; P=posterior; M=medial; L=lateral.

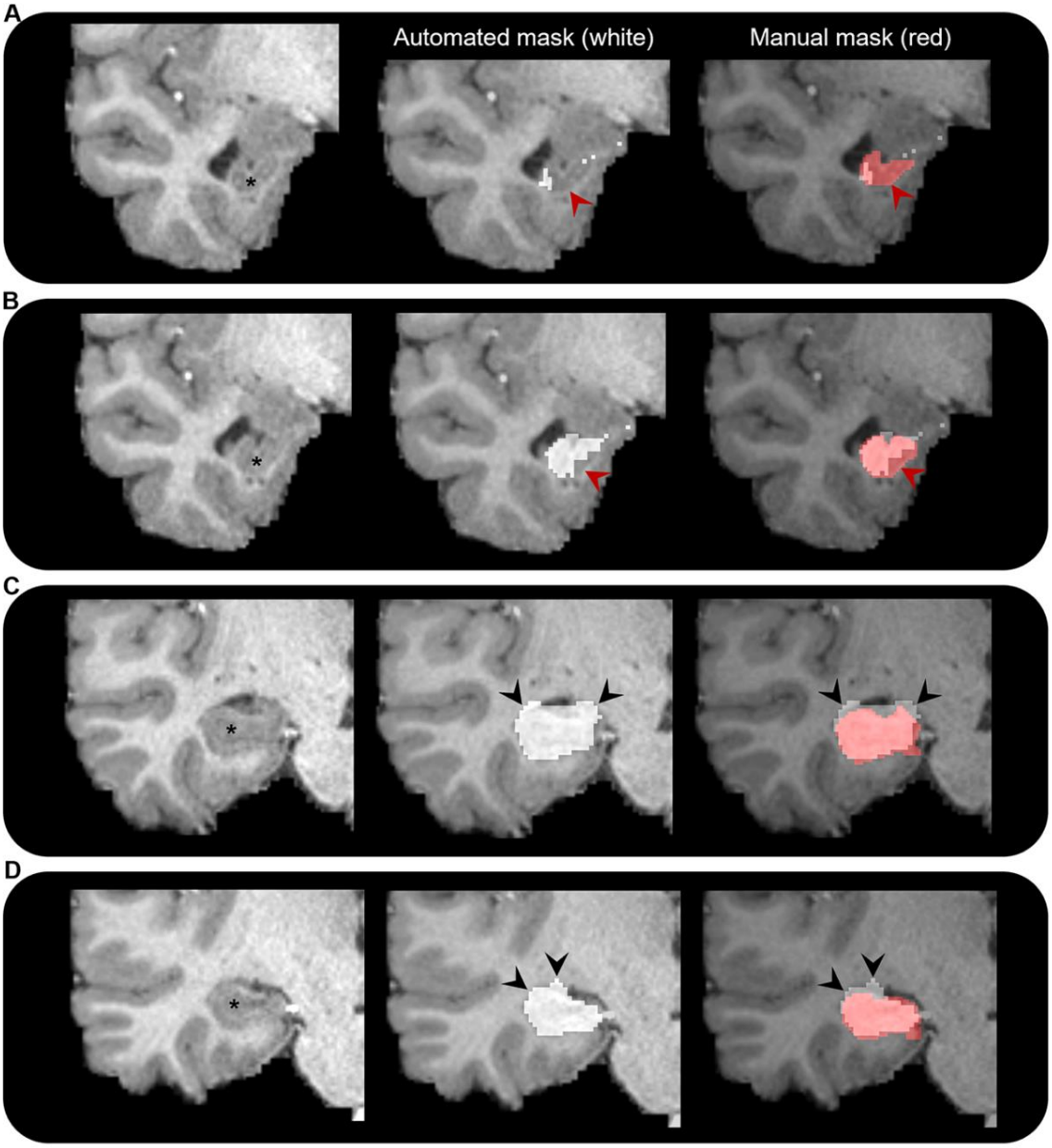

Fig. S6. Comparison of automated and manual hippocampus segmentations. Representative examples of the automated hippocampus mask derived from the HCPMMP and the manually segmented hippocampus mask. We display examples from anterior (a) to posterior (d) portions of the hippocampal head. In each panel, we present a coronal slice of the T1-weighted image focussed on the right temporal lobe for a single participant (left; hippocampus indicated by *), the same image overlaid with the automated hippocampus mask derived from the HCPMMP (middle; white) and the same image overlaid with both the automated HCPMMP hippocampus mask (right; white) and the manually segmented hippocampus mask (transparent red). Note, in the anterior most slices (a and b) the automated mask does not cover the entire extent of the hippocampus (indicated by red arrows) and in more posterior slices (c and d) the automated mask often overextends across the lateral ventricle superior to the hippocampus and into the adjacent white matter (indicated by black arrows). Streamlines making contact with these erroneous portions of the automated hippocampus mask may lead to results that are biologically implausible.

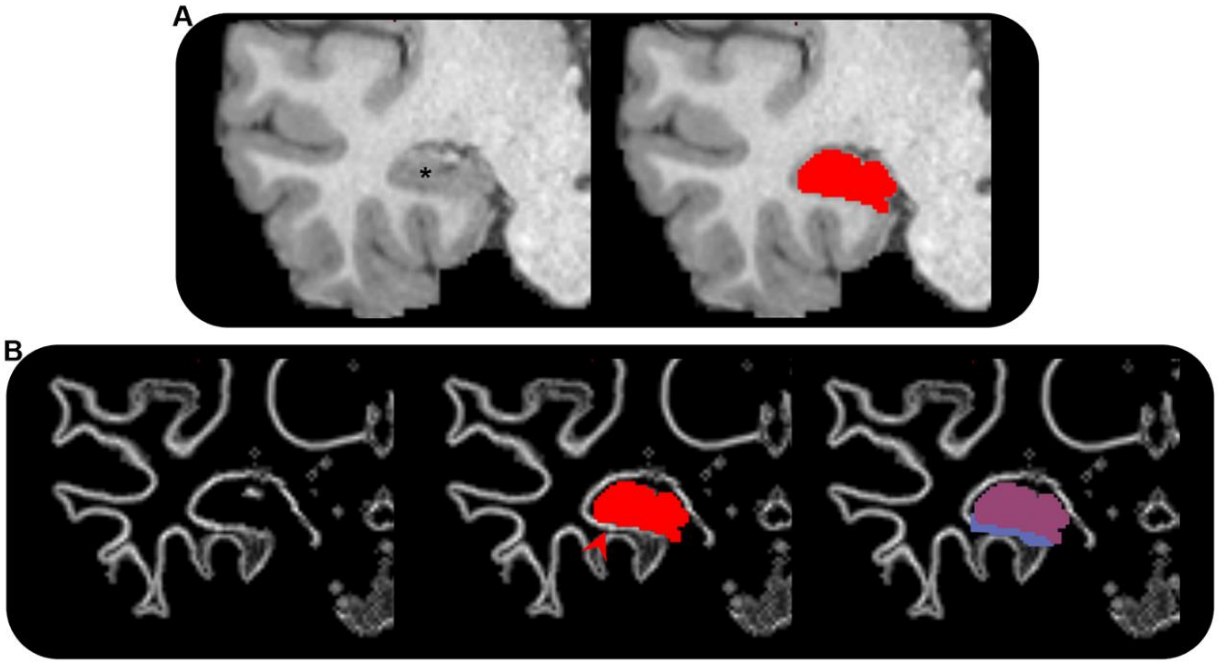

Fig. S7. Adjustment of grey matter/white matter interface underlying the hippocampus. a. T1-weighted structural MRI scan showing the right medial temporal lobe (left; hippocampus indicated by *) in the coronal plane for a single participant and the manually segmented hippocampus mask (red) overlaid on the T1-weighted image (right). b. (left) The grey matter/white matter (gm-wm) interface (white line) showing the right medial temporal lobe in the coronal plane; (middle) the manually segmented hippocampus mask (red) overlaid on the gm-wm interface. Note: portions of detected gm-wm interface immediately inferior to the hippocampus lie outside of the hippocampus mask (indicated by red arrow). If left unchanged, the anatomically-informed tractography algorithm used in our study would terminate tracks as they reach this band, thus creating an erroneous band of track end-points in this region, introducing misleading results. (Right) The hippocampus mask (transparent red) and extended hippocampus mask (blue) overlaid on the gm-wm interface. Note: the extended hippocampus mask encompasses the gm-wm interface immediately inferior to the hippocampus. This allows streamlines to enter/leave the hippocampus here rather than terminate at the gm-wm interface (see Methods for detail).

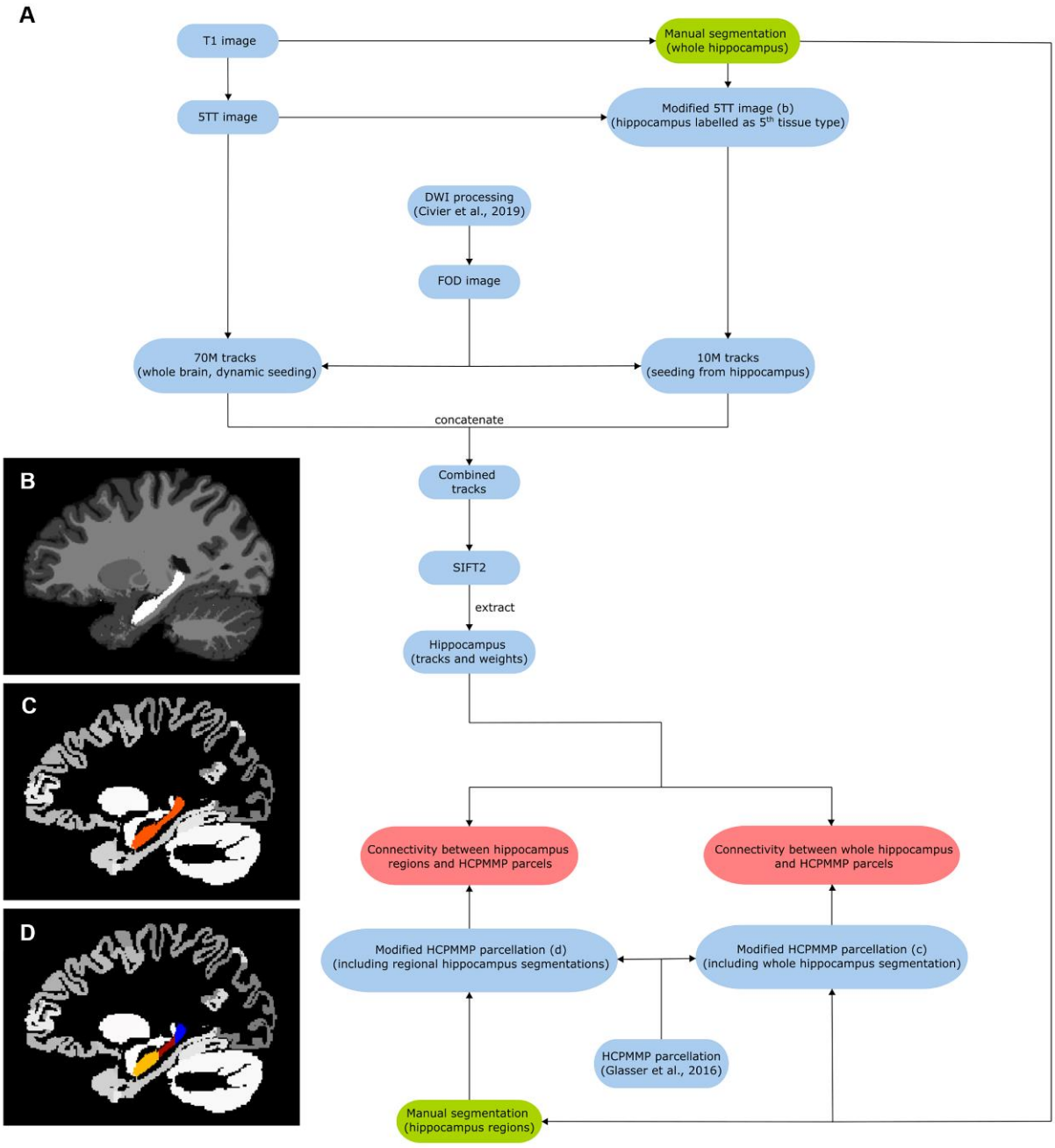

Fig. S8. Analysis pipeline. a. Block diagram of the workflow. Green blocks indicate procedures that involved manual segmentation, red blocks indicate connectivity vectors/matrices from which connectivity measurements were obtained and blue blocks indicate intermediate images. b. Sagittal view of 'modified 5TT' image containing the manually segmented hippocampus labelled as '5th tissue type' (i.e. no anatomical prior for tracking) shown in white. c. Sagittal view of modified parcellation image containing the whole-hippocampus mask (shown in orange). d. Sagittal view of modified parcellation image containing the regional hippocampus masks (head, body and tail shown in yellow, red and blue, respectively).

Table S1. Connectivity values between the cortical mantle and the whole hippocampus. Connectivity values between the whole hippocampus and all cortical areas in the Human Connectome Project Multi-Modal Parcellation (HCPMMP) scheme are presented. Column 1 displays each broad brain region ordered by their strength of connectivity with the whole hippocampus. Column 2 displays the percent of all cortical connections accounted for by each region. Values in brackets indicate the percent of cortical connections accounted for by each region when excluding medial temporal lobe (MTL) areas. Column 3 presents the cortical areas located within each broad brain region ordered by their strength of connectivity with the whole hippocampus (abbreviations for all cortical areas are defined in Table S3). Column 4 displays the mean SIFT2 weighted value (connectivity strength) associated with each cortical area. Column 5 displays the standard error of the mean. Column 6 displays the percent of all cortical connections accounted for by each cortical area. Values in brackets indicate the percent of cortical connections accounted for by each cortical area when excluding MTL areas. Column 7 displays the rank order for each cortical area by strength of connectivity. Values in brackets indicate the rank order when excluding MTL areas.

Brain region	Percent of all cortical connections accounted for by region. (Percent of cortical connections excluding medial temporal areas)	Cortical areas within each brain region	Mean SIFT2 weighted value (connectivity strength; n=10)	SE of mean	Percent of all cortical connections accounted for by area. (Percent of cortical connections excluding MTL areas)	Rank order for each cortical area by strength of connectivity (Rank order for each cortical area excluding MTL areas)
Medial Temporal Cortex	52.0 (N/A)	EC	35585	3509	23.64 (N/A)	1 (N/A)
		PeEc	21683	2377	14.40 (N/A)	2 (N/A)
		PHA2	8603	854	5.72 (N/A)	3 (N/A)
		PHA1	7902	887	5.25 (N/A)	4 (N/A)
		PHA3	4447	359	2.95 (N/A)	8 (N/A)
Lateral Temporal Cortex (including Temporal Pole)	13.3 (27.8)	TF	7673	886	5.10 (10.61)	5 (1)
		TGd	3465	288	2.30 (4.79)	11 (6)
		TGv	3337	313	2.22 (4.61)	12 (7)
		TE2a	2214	288	1.47 (3.06)	14 (9)
		TE2p	1288	198	0.86 (1.78)	23 (18)
		TE1a	694	96	0.46 (0.96)	29 (24)
		TE1p	676	99	0.45 (0.93)	30 (25)
		TE1m	461	77	0.31 (0.64)	33 (28)

		PHT	265	34	0.18 (0.37)	41 (36)
Medial Parietal Cortex (including Posterior Cingulate)	11.3 (23.5)	ProS	5483	784	3.64 (7.58)	6 (2)
		POS1	3712	424	2.47 (5.13)	10 (5)
		RSC	2063	121	1.37 (2.85)	16 (11)
		DVT	1939	335	1.29 (2.68)	18 (13)
		POS2	1802	248	1.20 (2.49)	19 (14)
		7m	696	96	0.46 (0.96)	28 (23)
		v23ab	565	85	0.38 (0.78)	31 (26)
		d23ab	178	12	0.12 (0.25)	55 (50)
		31pd	156	22	0.10 (0.22)	62 (57)
		PCV	130	24	0.09 (0.18)	66 (61)
		31pv	87	8	0.06 (0.12)	74 (69)
		23d	47	6	0.03 (0.06)	89 (84)
		23c	42	5	0.03 (0.06)	93 (88)
		31a	41	5	0.03 (0.06)	94 (89)
Early Visual Cortex (Occipital)	9.2 (19.2)	V1	5385	579	3.58 (7.45)	7 (3)
		V2	3840	462	2.55 (5.31)	9 (4)
		V3	3079	450	2.05 (4.26)	13 (8)
		V4	1601	127	1.06 (2.21)	22 (17)
Ventral Stream Visual Cortex	6.1 (12.7)	VMV2	2105	247	1.40 (2.91)	15 (10)
		VVC	1956	220	1.30 (2.71)	17 (12)
		VMV1	1788	248	1.19 (2.47)	20 (15)
		FFC	1670	172	1.11 (2.31)	21 (16)
		VMV3	819	34	0.54 (1.13)	26 (21)
		V8	516	53	0.34 (0.71)	32 (27)
		PIT	326	51	0.22 (0.45)	40 (35)
	2.2	V6	1050	195	0.70 (1.45)	24 (19)

Dorsal Stream Visual Cortex	(4.5)	V3A	1029	197	0.68 (1.42)	25 (20)
		IPS1	358	37	0.24 (0.50)	37 (32)
		V7	334	40	0.22 (0.46)	38 (33)
		V6A	331	52	0.22 (0.46)	39 (34)
		V3B	176	23	0.12 (0.24)	58 (53)
MT+ Complex and Neighbouring Visual Areas	1.5 (3.2)	PH	779	86	0.52 (1.08)	27 (22)
		V3CD	234	31	0.16 (0.32)	45 (40)
		FST	231	25	0.15 (0.32)	46 (41)
		LO2	201	33	0.13 (0.28)	49 (44)
		LO3	183	22	0.12 (0.25)	51 (46)
		V4t	182	31	0.12 (0.25)	52 (47)
		MST	177	21	0.12 (0.24)	56 (51)
		MT	177	22	0.12 (0.24)	57 (52)
		LO1	132	24	0.09 (0.18)	65 (60)
Inferior Parietal Cortex	1.0 (2.0)	PGp	414	33	0.28 (0.57)	34 (29)
		PGs	249	36	0.17 (0.34)	43 (38)
		PGi	181	21	0.12 (0.25)	53 (48)
		PFm	179	27	0.12 (0.25)	54 (49)
		IP0	173	14	0.11 (0.24)	60 (55)
		IP1	118	11	0.08 (0.16)	68 (63)
		PF	59	10	0.04 (0.08)	81 (76)
		IP2	33	6	0.02 (0.05)	105 (100)
		PFt	13	2	0.01 (0.02)	126 (121)
		PFop	10	1	0.01 (0.01)	132 (127)
Auditory Association Cortex	0.9 (1.8)	STSva	403	40	0.27 (0.56)	36 (31)
		STSvp	238	30	0.16 (0.33)	44 (39)
		STSda	195	21	0.13 (0.27)	50 (45)

		STSdp	176	34	0.12 (0.24)	59 (54)
		STGa	96	13	0.06 (0.13)	71 (66)
		A5	91	14	0.06 (0.13)	73 (68)
		A4	78	13	0.05 (0.11)	76 (71)
		TA2	33	6	0.02 (0.05)	106 (101)
Insular and Frontal Opercular Cortex	0.7 (1.5)	PoI1	408	86	0.27 (0.56)	35 (30)
		Pir	259	37	0.17 (0.36)	42 (37)
		PI	202	28	0.13 (0.28)	48 (43)
		52	99	12	0.07 (0.14)	70 (65)
		AAIC	36	6	0.02 (0.05)	100 (95)
		PoI2	36	8	0.02 (0.05)	101 (96)
		Ig	6	1	< 0.01 (0.01)	145 (140)
		MI	6	2	< 0.01 (0.01)	146 (141)
		FOP4	4	1	< 0.01 (0.01)	156 (151)
		AVI	3	1	< 0.01 (< 0.01)	163 (158)
		FOP5	2	1	< 0.01 (< 0.01)	170 (165)
		FOP3	2	0	< 0.01 (< 0.01)	171 (166)
		FOP2	2	0	< 0.01 (< 0.01)	172 (167)
Superior Parietal Cortex	0.7 (1.4)	7Pm	216	41	0.14 (0.30)	47 (42)
		7PL	160	27	0.11 (0.22)	61 (56)
		MIP	149	20	0.10 (0.21)	63 (58)
		7Am	139	23	0.09 (0.19)	64 (59)
		VIP	81	13	0.05 (0.11)	75 (70)
		7AL	78	15	0.05 (0.11)	77 (72)
		LIPv	73	14	0.05 (0.10)	79 (74)
		7PC	48	9	0.03 (0.07)	87 (82)
		LIPd	38	7	0.03 (0.05)	99 (94)

		AIP	20	3	0.01 (0.03)	116 (111)
Temporo-Parieto-Occipital Junction	0.3 (0.6)	TPOJ3	130	12	0.09 (0.18)	67 (62)
		TPOJ2	104	11	0.07 (0.14)	69 (64)
		TPOJ1	96	13	0.06 (0.13)	72 (67)
		PSL	51	5	0.03 (0.07)	83 (78)
		STV	48	6	0.03 (0.07)	88 (83)
Anterior Cingulate and Medial Prefrontal Cortex	0.3 (0.6)	33pr	75	10	0.05 (0.10)	78 (73)
		a24pr	49	6	0.03 (0.07)	84 (79)
		p32pr	49	8	0.03 (0.07)	85 (80)
		a32pr	46	8	0.03 (0.06)	90 (85)
		8BM	41	6	0.03 (0.06)	95 (90)
		p24pr	41	4	0.03 (0.06)	96 (91)
		p24	35	6	0.02 (0.05)	102 (97)
		9m	31	6	0.02 (0.04)	109 (104)
		d32	28	5	0.02 (0.04)	111 (106)
		a24	14	3	< 0.01 (0.02)	125 (120)
		p32	5	1	< 0.01 (0.01)	153 (148)
		10r	3	0	< 0.01 (< 0.01)	164 (159)
		10v	2	1	< 0.01 (< 0.01)	173 (168)
		25	2	1	< 0.01 (< 0.01)	174 (169)
		s32	2	0	< 0.01 (< 0.01)	175 (170)
Somatosensory and Motor Cortex	0.2 (0.3)	4	62	9	0.04 (0.09)	80 (75)
		2	55	8	0.04 (0.08)	82 (77)
		1	39	7	0.03 (0.05)	98 (93)
		3b	33	5	0.02 (0.05)	107 (102)
		3a	21	4	0.01 (0.03)	114 (109)
		5m	11	2	< 0.01 (0.02)	129 (124)

Early Auditory Cortex	0.1 (0.3)	PBelt	49	8	0.03 (0.07)	86 (81)
		LBelt	45	6	0.02 (0.06)	91 (86)
		MBelt	43	7	0.02 (0.06)	92 (87)
		RI	35	3	0.02 (0.05)	103 (98)
		A1	30	4	0.02 (0.04)	110 (105)
Paracentral Lobular and Mid Cingulate Cortex	0.1 (0.3)	5mv	40	6	0.03 (0.06)	97 (92)
		5L	34	9	0.02 (0.05)	104 (99)
		SCEF	32	5	0.02 (0.04)	108 (103)
		6mp	27	5	0.02 (0.04)	112 (107)
		6ma	26	4	0.02 (0.04)	113 (108)
		24dv	20	7	0.01 (0.03)	117 (112)
		24dd	17	3	0.01 (0.02)	121 (116)
Dorsolateral Prefrontal Cortex	< 0.1 (0.2)	SFL	21	3	0.01 (0.03)	115 (110)
		8BL	19	3	0.01 (0.03)	118 (113)
		8Av	17	3	0.01 (0.02)	122 (117)
		8C	10	2	0.01 (0.01)	133 (128)
		i6-8	10	2	0.01 (0.01)	134 (129)
		9p	9	2	0.01 (0.01)	135 (130)
		9a	8	1	0.01 (0.01)	136 (131)
		9-46d	7	1	< 0.01 (0.01)	140 (135)
		8Ad	7	1	< 0.01 (0.01)	141 (136)
		46	7	1	< 0.01 (0.01)	142 (137)
		s6-8	7	1	< 0.01 (0.01)	143 (138)
		p9-46v	6	1	< 0.01 (0.01)	147 (142)
		a9-46v	4	1	< 0.01 (0.01)	157 (152)
Premotor Cortex	< 0.1 (0.1)	6r	19	3	0.01 (0.03)	119 (114)
		6a	16	2	0.01 (0.02)	123 (118)

		6d	16	3	0.01 (0.02)	124 (119)
		6v	13	2	0.01 (0.02)	127 (122)
		FEF	11	2	0.01 (0.02)	130 (125)
		55b	11	2	0.01 (0.02)	131 (126)
		PEF	6	1	< 0.01 (0.01)	148 (143)
Orbital and Polar Frontal Cortex	< 0.1 (< 0.1)	10d	8	2	0.01 (0.01)	137 (132)
		a47r	6	2	< 0.01 (0.01)	149 (144)
		47s	6	1	< 0.01 (0.01)	150 (145)
		13l	4	1	< 0.01 (0.01)	158 (153)
		pOFC	4	1	< 0.01 (0.01)	159 (154)
		p10p	4	1	< 0.01 (0.01)	160 (155)
		OFC	4	1	< 0.01 (0.01)	161 (156)
		10pp	3	1	< 0.01 (< 0.01)	165 (160)
		11l	3	1	< 0.01 (< 0.01)	166 (161)
		a10p	2	1	< 0.01 (< 0.01)	176 (171)
		47m	2	0	< 0.01 (< 0.01)	177 (172)
Inferior Frontal Cortex	< 0.1 (< 0.1)	44	12	2	0.01 (0.02)	128 (123)
		IFJa	8	1	0.01 (0.01)	138 (133)
		IFSp	7	1	< 0.01 (0.01)	144 (139)
		IFSa	5	1	< 0.01 (0.01)	154 (149)
		45	5	1	< 0.01 (0.01)	155 (150)
		IFJp	3	1	< 0.01 (< 0.01)	167 (162)
		p47r	3	1	< 0.01 (< 0.01)	168 (163)
		47l	2	1	< 0.01 (< 0.01)	178 (173)
Posterior Opercular Cortex	< 0.1 (< 0.1)	PFcm	18	3	0.01 (0.02)	120 (115)
		OP1	8	2	0.01 (0.01)	139 (134)
		OP4	6	1	< 0.01 (0.01)	151 (146)

		43	6	1	< 0.01 (0.01)	152 (147)
		OP2-3	4	1	< 0.01 (0.01)	162 (157)
		FOP1	3	1	< 0.01 (< 0.01)	169 (164)

Table S2. Connectivity between the cortical mantle and the head, body and tail of the hippocampus. Connectivity values between the head, body and tail of the hippocampus and all cortical brain areas included in the Human Connectome Project Multi-Modal Parcellation (HCPMMP) scheme are presented. Column 1 displays each cortical area ordered by strength of connectivity with the whole hippocampus (abbreviations for all cortical areas are defined in Table S3). Column 2 presents the broader brain region within which each cortical area is located. Column 3 displays the mean SIFT2 weighted value (connectivity strength) associated with each cortical area and the head of the hippocampus. Column 4 displays the associated standard error of the mean. Column 5 displays the mean SIFT2 weighted value (connectivity strength) associated with each cortical area and the body of the hippocampus. Column 6 displays the associated standard error of the mean. Column 7 displays the mean SIFT2 weighted value (connectivity strength) associated with each cortical area and the tail of the hippocampus. Column 8 displays the associated standard error of the mean.

Cortical area	Location of area	Head		Body		Tail	
		Mean SIFT2 weighted value (n=10)	SE of Mean	Mean SIFT2 weighted value (n=10)	SE of Mean	Mean SIFT2 weighted value (n=10)	SE of Mean
EC	Medial Temporal Cortex	16206	1927	12679	1357	6700	843
PeEc	Medial Temporal Cortex	11144	1414	7838	998	2700	366
PHA2	Medial Temporal Cortex	2644	322	4545	566	1414	116
PHA1	Medial Temporal Cortex	2287	299	3716	450	1899	243
TF	Lateral Temporal Cortex	3287	500	3452	410	934	144
ProS	Medial Parietal Cortex (including Posterior Cingulate)	716	116	1625	194	3143	553
V1	Early Visual Cortex (Occipital)	567	70	1389	112	3429	489
PHA3	Medial Temporal Cortex	1420	134	2277	236	750	76
V2	Early Visual Cortex (Occipital)	428	62	1054	82	2358	376
POS1	Medial Parietal Cortex (including Posterior Cingulate)	620	89	1299	112	1793	297
TGd	Lateral Temporal Cortex	1576	182	1446	117	443	47
TGv	Lateral Temporal Cortex	1589	207	1358	144	389	41
V3	Early Visual Cortex (Occipital)	327	37	810	83	1942	357
TE2a	Lateral Temporal Cortex	754	132	1038	107	422	65
VMV2	Ventral Stream Visual Cortex	354	68	860	111	891	97
RSC	Medial Parietal Cortex (including Posterior Cingulate)	401	55	733	52	928	107

VVC	Ventral Stream Visual Cortex	460	76	969	129	528	48
DVT	Medial Parietal Cortex (including Posterior Cingulate)	247	36	515	65	1178	253
POS2	Medial Parietal Cortex (including Posterior Cingulate)	303	32	590	47	909	195
VMV1	Ventral Stream Visual Cortex	245	47	644	115	899	110
FFC	Ventral Stream Visual Cortex	355	49	798	109	517	55
V4	Early Visual Cortex (Occipital)	183	20	472	40	946	116
TE2p	Lateral Temporal Cortex	348	69	658	101	282	45
V6	Dorsal Stream Visual Cortex	113	16	259	37	678	149
V3A	Dorsal Stream Visual Cortex	103	11	252	35	674	155
VMV3	Ventral Stream Visual Cortex	127	16	306	28	386	23
PH	MT+ Complex and Neighbouring Visual Areas	136	18	338	44	305	40
7m	Medial Parietal Cortex (including Posterior Cingulate)	120	17	251	26	325	69
TE1a	Lateral Temporal Cortex	209	42	329	39	156	23
TE1p	Lateral Temporal Cortex	146	27	334	46	196	32
v23ab	Medial Parietal Cortex (including Posterior Cingulate)	91	14	207	23	267	60
V8	Ventral Stream Visual Cortex	72	14	178	20	265	33
TE1m	Lateral Temporal Cortex	121	32	232	35	108	14
PGp	Inferior Parietal Cortex	58	7	147	12	209	25
PoI1	Insular and Frontal Opercular Cortex	110	21	174	36	124	31
STSva	Auditory Association Cortex	108	17	198	17	98	9
IPS1	Dorsal Stream Visual Cortex	38	6	100	6	220	27
V7	Dorsal Stream Visual Cortex	38	6	88	6	207	32
V6A	Dorsal Stream Visual Cortex	45	8	92	14	194	33
PIT	Ventral Stream Visual Cortex	41	8	116	26	168	25
PHT	Lateral Temporal Cortex	52	10	127	15	86	13
Pir	Insular and Frontal Opercular Cortex	148	27	81	10	29	4
PGs	Inferior Parietal Cortex	37	8	100	13	112	17

STSvp	Auditory Association Cortex	46	8	122	15	70	9
V3CD	MT+ Complex and Neighbouring Visual Areas	20	3	65	7	149	26
FST	MT+ Complex and Neighbouring Visual Areas	34	5	92	13	105	14
7Pm	Superior Parietal Cortex	43	9	77	16	96	19
PI	Insular and Frontal Opercular Cortex	55	12	89	9	58	9
LO2	MT+ Complex and Neighbouring Visual Areas	23	3	65	11	113	24
STSda	Auditory Association Cortex	54	10	90	9	51	5
LO3	MT+ Complex and Neighbouring Visual Areas	21	3	66	9	97	16
V4t	MT+ Complex and Neighbouring Visual Areas	24	5	62	13	96	18
PGi	Inferior Parietal Cortex	27	5	85	14	70	8
PFm	Inferior Parietal Cortex	27	6	80	11	73	12
d23ab	Medial Parietal Cortex (including Posterior Cingulate)	28	4	62	5	88	8
MST	MT+ Complex and Neighbouring Visual Areas	21	3	71	10	86	14
MT	MT+ Complex and Neighbouring Visual Areas	21	3	64	9	92	15
V3B	Dorsal Stream Visual Cortex	13	2	43	4	120	21
STSdp	Auditory Association Cortex	37	12	84	13	55	10
IP0	Inferior Parietal Cortex	18	2	56	3	99	12
7PL	Superior Parietal Cortex	28	6	58	11	73	11
31pd	Medial Parietal Cortex (including Posterior Cingulate)	25	5	55	6	76	14
MIP	Superior Parietal Cortex	17	4	52	8	80	10
7Am	Superior Parietal Cortex	23	4	53	9	63	12
LO1	MT+ Complex and Neighbouring Visual Areas	12	3	38	8	83	18
PCV	Medial Parietal Cortex (including Posterior Cingulate)	23	5	47	9	60	13
TPOJ3	Temporo-Parieto-Occipital Junction	15	2	51	4	64	10
IP1	Inferior Parietal Cortex	15	3	43	3	60	7
TPOJ2	Temporo-Parieto-Occipital Junction	16	3	48	6	40	5
52	Insular and Frontal Opercular Cortex	18	2	41	3	40	8

TPOJ1	Temporo-Parieto-Occipital Junction	17	3	46	5	34	6
STGa	Auditory Association Cortex	31	7	45	5	19	3
A5	Auditory Association Cortex	19	3	39	4	32	7
31pv	Medial Parietal Cortex (including Posterior Cingulate)	14	2	32	3	41	5
VIP	Superior Parietal Cortex	12	3	31	5	38	5
7AL	Superior Parietal Cortex	10	2	30	5	38	8
A4	Auditory Association Cortex	14	3	34	4	30	6
33pr	Anterior Cingulate and Medial Prefrontal Cortex	14	2	28	4	33	5
LIPv	Superior Parietal Cortex	8	2	28	5	37	8
4	Somatosensory and Motor Cortex	8	2	28	5	26	5
PF	Inferior Parietal Cortex	11	3	27	5	21	3
2	Somatosensory and Motor Cortex	7	1	25	4	23	3
PSL	Temporo-Parieto-Occipital Junction	9	1	24	3	18	2
a24pr	Anterior Cingulate and Medial Prefrontal Cortex	10	2	18	2	21	3
p32pr	Anterior Cingulate and Medial Prefrontal Cortex	12	3	18	3	20	4
PBelt	Early Auditory Cortex	9	2	21	2	19	4
7PC	Superior Parietal Cortex	6	2	20	4	22	4
STV	Temporo-Parieto-Occipital Junction	7	2	23	3	18	3
23d	Medial Parietal Cortex (including Posterior Cingulate)	7	1	18	3	22	3
a32pr	Anterior Cingulate and Medial Prefrontal Cortex	11	3	18	3	17	3
LBelt	Early Auditory Cortex	7	1	19	2	19	3
MBelt	Early Auditory Cortex	6	1	19	2	17	4
23c	Medial Parietal Cortex (including Posterior Cingulate)	6	1	15	2	21	3
8BM	Anterior Cingulate and Medial Prefrontal Cortex	10	2	16	3	15	3
p24pr	Anterior Cingulate and Medial Prefrontal Cortex	7	1	15	2	19	3
31a	Medial Parietal Cortex (including Posterior Cingulate)	7	2	14	1	20	3
5mv	Paracentral Lobular and Mid Cingulate Cortex	5	1	15	2	20	4

1	Somatosensory and Motor Cortex	4	1	19	3	16	3
LIPd	Superior Parietal Cortex	4	1	14	3	20	4
AAIC	Insular and Frontal Opercular Cortex	12	4	17	3	7	1
PoI2	Insular and Frontal Opercular Cortex	13	5	14	3	8	1
p24	Anterior Cingulate and Medial Prefrontal Cortex	7	2	13	2	15	2
RI	Early Auditory Cortex	4	1	18	1	13	2
5L	Paracentral Lobular and Mid Cingulate Cortex	5	1	12	3	17	4
3b	Somatosensory and Motor Cortex	3	1	15	3	15	3
TA2	Auditory Association Cortex	8	2	15	3	11	2
IP2	Inferior Parietal Cortex	4	1	14	3	15	3
SCEF	Paracentral Lobular and Mid Cingulate Cortex	5	1	13	2	14	3
9m	Anterior Cingulate and Medial Prefrontal Cortex	8	2	12	3	11	2
A1	Early Auditory Cortex	4	1	12	1	13	3
d32	Anterior Cingulate and Medial Prefrontal Cortex	7	1	10	2	11	2
6mp	Paracentral Lobular and Mid Cingulate Cortex	3	1	12	3	12	2
6ma	Paracentral Lobular and Mid Cingulate Cortex	3	1	10	2	13	2
SFL	DorsoLateral Prefrontal Cortex	4	1	7	1	10	2
3a	Somatosensory and Motor Cortex	2	1	11	2	8	1
AIP	Superior Parietal Cortex	3	1	8	1	10	2
24dv	Paracentral Lobular and Mid Cingulate Cortex	4	2	6	2	10	4
6r	Premotor Cortex	3	1	9	1	6	1
8BL	DorsoLateral Prefrontal Cortex	4	1	7	2	8	1
PFcm	Posterior Opercular Cortex	3	1	8	1	7	1
8Av	DorsoLateral Prefrontal Cortex	3	1	7	1	7	1
24dd	Paracentral Lobular and Mid Cingulate Cortex	2	0	6	1	8	2
6a	Premotor Cortex	2	0	7	1	7	1
6d	Premotor Cortex	2	1	8	2	6	1

a24	Anterior Cingulate and Medial Prefrontal Cortex	3	1	5	1	6	2
6v	Premotor Cortex	2	1	6	1	5	1
PFt	Inferior Parietal Cortex	2	1	7	1	4	1
44	Inferior Frontal Cortex	2	1	5	1	4	1
FEF	Premotor Cortex	2	1	5	1	5	1
5m	Somatosensory and Motor Cortex	2	0	4	1	5	1
55b	Premotor Cortex	2	0	5	1	4	1
PFop	Inferior Parietal Cortex	2	0	5	1	4	1
8C	DorsoLateral Prefrontal Cortex	2	0	5	1	3	1
i6-8	DorsoLateral Prefrontal Cortex	2	0	4	1	4	1
9p	DorsoLateral Prefrontal Cortex	1	0	4	1	4	1
10d	Orbital and Polar Frontal Cortex	2	1	3	1	3	1
9a	DorsoLateral Prefrontal Cortex	1	0	3	1	4	1
OP1	Posterior Opercular Cortex	1	0	4	1	2	1
IFJa	Inferior Frontal Cortex	2	0	3	1	3	1
9-46d	DorsoLateral Prefrontal Cortex	1	0	2	0	4	0
8Ad	DorsoLateral Prefrontal Cortex	1	0	2	0	4	1
46	DorsoLateral Prefrontal Cortex	1	0	3	1	3	1
IFSp	Inferior Frontal Cortex	1	0	3	1	2	0
s6-8	DorsoLateral Prefrontal Cortex	1	0	2	0	4	1
p9-46v	DorsoLateral Prefrontal Cortex	1	0	2	1	3	1
OP4	Posterior Opercular Cortex	1	1	3	1	2	0
a47r	Orbital and Polar Frontal Cortex	1	0	2	1	3	1
43	Posterior Opercular Cortex	1	0	3	0	2	0
Ig	Insular and Frontal Opercular Cortex	1	0	3	0	2	0
MI	Insular and Frontal Opercular Cortex	1	0	3	1	2	1
47s	Orbital and Polar Frontal Cortex	1	0	3	1	2	1

PEF	Premotor Cortex	1	0	2	0	2	1
p32	Anterior Cingulate and Medial Prefrontal Cortex	1	0	2	0	2	1
IFSa	Inferior Frontal Cortex	1	0	2	0	2	0
45	Inferior Frontal Cortex	1	0	2	0	2	0
13l	Orbital and Polar Frontal Cortex	1	0	2	1	1	0
pOFC	Orbital and Polar Frontal Cortex	1	0	2	1	1	0
FOP4	Insular and Frontal Opercular Cortex	1	0	2	0	2	0
p10p	Orbital and Polar Frontal Cortex	1	0	1	0	2	0
OFC	Orbital and Polar Frontal Cortex	1	0	2	1	1	0
a9-46v	DorsoLateral Prefrontal Cortex	1	0	2	0	1	0
OP2-3	Posterior Opercular Cortex	1	0	2	0	1	0
FOP1	Posterior Opercular Cortex	0	0	2	1	1	0
IFJp	Inferior Frontal Cortex	1	0	1	0	1	0
p47r	Inferior Frontal Cortex	1	0	1	0	1	0
10r	Anterior Cingulate and Medial Prefrontal Cortex	1	0	1	0	1	0
10pp	Orbital and Polar Frontal Cortex	1	0	1	0	1	0
AVI	Insular and Frontal Opercular Cortex	1	0	1	1	1	0
11l	Orbital and Polar Frontal Cortex	1	0	1	0	1	0
10v	Anterior Cingulate and Medial Prefrontal Cortex	1	0	1	0	1	0
47l	Inferior Frontal Cortex	0	0	1	0	1	0
a10p	Orbital and Polar Frontal Cortex	0	0	1	0	1	0
FOP5	Insular and Frontal Opercular Cortex	0	0	1	0	1	1
25	Anterior Cingulate and Medial Prefrontal Cortex	0	0	1	0	1	0
FOP3	Insular and Frontal Opercular Cortex	0	0	1	0	1	0
FOP2	Insular and Frontal Opercular Cortex	0	0	1	0	1	0
47m	Orbital and Polar Frontal Cortex	0	0	1	0	1	0
s32	Anterior Cingulate and Medial Prefrontal Cortex	0	0	1	0	0	0

Table S3. List of abbreviations for all cortical brain areas in the Human Connectome Project Multi-Modal Parcellation (HCPMMP) scheme.

Brain region	Cortical areas within each brain region	
Medial Temporal Cortex	EC	Entorhinal Cortex
	PeEc	Perirhinal Ectorhinal Cortex
	PHA1	ParaHippocampal Area 1
	PHA2	ParaHippocampal Area 2
	PHA3	ParaHippocampal Area 3
Lateral Temporal Cortex (including Temporal Pole)	PHT	Area PHT
	TE1a	Area TE1 anterior
	TE1m	Area TE1 Middle
	TE1p	Area TE1 posterior
	TE2a	Area TE2 anterior
	TE2p	Area TE2 posterior
	TF	Area TF
	TGd	Area TG dorsal
	TGv	Area TG Ventral
Medial Parietal Cortex (including Posterior Cingulate)	23c	Area 23c
	23d	Area 23d
	31a	Area 31a
	31pd	Area 31pd
	31pv	Area 31p ventral
	7m	Area 7m
	d23ab	Area dorsal 23 a+b
	DVT	Dorsal Transitional Visual Area
	PCV	PreCuneus Visual Area
	POS1	Parieto-Occipital Sulcus Area 1
	POS2	Parieto-Occipital Sulcus Area 2
	ProS	ProStriate Area
	RSC	RetroSplenial Complex
	v23ab	Area ventral 23 a+b
Early Visual Cortex (Occipital)	V1	Primary Visual Cortex
	V2	Second Visual Area
	V3	Third Visual Area
	V4	Fourth Visual Area
Ventral Stream Visual Cortex	FFC	Fusiform Face Complex
	PIT	Posterior InferoTemporal Complex
	V8	Eighth Visual Area
	VMV1	VentroMedial Visual Area 1

	VMV2	VentroMedial Visual Area 2
	VMV3	VentroMedial Visual Area 3
	VVC	Ventral Visual Complex
Dorsal Stream Visual Cortex	IPS1	IntraParietal Sulcus Area 1
	V3A	Area V3A
	V3B	Area V3B
	V6	Sixth Visual Area
	V6A	Area V6A
	V7	Seventh Visual Area
MT+ Complex and Neighbouring Visual Areas	FST	Area FST
	LO1	Area Lateral Occipital 1
	LO2	Area Lateral Occipital 2
	LO3	Area Lateral Occipital 3
	MST	Medial Superior Temporal Area
	MT	Middle Temporal Area
	PH	Area PH
	V3CD	Area V3CD
	V4t	Area V4t
Inferior Parietal Cortex	IP0	Area IntraParietal 0
	IP1	Area IntraParietal 1
	IP2	Area IntraParietal 2
	PF	Area PF Complex
	PFm	Area PFm Complex
	PFop	Area PF opercular
	PFt	Area PFt
	PGi	Area PGi
	PGp	Area PGp
	PGs	Area PGs
Auditory Association Cortex	A4	Auditory 4 Complex
	A5	Auditory 5 Complex
	STGa	Area STGa
	STSda	Area STSd anterior
	STSdp	Area STSd posterior
	STSva	Area STSv anterior
	STSvp	Area STSv posterior
	TA2	Area TA2
Insular and Frontal Opercular Cortex	52	Area 52
	AAIC	Anterior Agranular Insula Complex
	AVI	Anterior Ventral Insular Area
	FOP2	Frontal Opercular Area 2
	FOP3	Frontal Opercular Area 3

	FOP4	Frontal Opercular Area 4
	FOP5	Area Frontal Opercular 5
	Ig	Insular Granular Complex
	MI	Middle Insular Area
	PI	Para-Insular Area
	Pir	Pirform Cortex
	PoI1	Area Posterior Insular 1
	PoI2	Posterior Insular Area 2
Superior Parietal Cortex	7AL	Lateral Area 7A
	7Am	Medial Area 7A
	7PC	Area 7PC
	7PL	Lateral Area 7P
	7Pm	Medial Area 7P
	AIP	Anterior IntraParietal Area
	LIPd	Area Lateral IntraParietal dorsal
	LIPv	Area Lateral IntraParietal ventral
	MIP	Medial IntraParietal Area
	VIP	Ventral IntraParietal Complex
Temporo-Parieto-Occipital Junction	PSL	PeriSylvian Language Area
	STV	Superior Temporal Visual Area
	TPOJ1	Area TemporoParietoOccipital Junction 1
	TPOJ2	Area TemporoParietoOccipital Junction 2
	TPOJ3	Area TemporoParietoOccipital Junction 3
Anterior Cingulate and Medial Prefrontal Cortex	25	Area 25
	10r	Area 10r
	10v	Area 10v
	33pr	Area 33 prime
	8BM	Area 8BM
	9m	Area 9 Middle
	a24	Area a24
	a24pr	Anterior 24 prime
	a32pr	Area anterior 32 prime
	d32	Area dorsal 32
	p24	Area posterior 24
	p24pr	Area Posterior 24 prime
	p32	Area p32
	p32pr	Area p32 prime
	s32	Area s32
Somatosensory and Motor Cortex	1	Area 1
	2	Area 2
	4	Primary Motor Cortex

	3a	Area 3a
	3b	Primary Sensory Cortex
	5m	Area 5m
Early Auditory Cortex	A1	Primary Auditory Cortex
	LBelt	Lateral Belt Complex
	MBelt	Medial Belt Complex
	PBelt	ParaBelt Complex
	RI	RetroInsular Cortex
Paracentral Lobular and Mid Cingulate Cortex	24dd	Dorsal Area 24d
	24dv	Ventral Area 24d
	5mv	Area 5m ventral
	5L	Area 5L
	6ma	Area 6m anterior
	6mp	Area 6mp
	SCEF	Supplementary and Cingulate Eye Field
Dorsolateral Prefrontal Cortex	46	Area 46
	8Ad	Area 8Ad
	8Av	Area 8Av
	8BL	Area 8B Lateral
	8C	Area 8C
	9-46d	Area 9-46d
	9a	Area 9 anterior
	9p	Area 9 Posterior
	a9-46v	Area anterior 9-46v
	i6-8	Inferior 6-8 Transitional Area
	p9-46v	Area posterior 9-46v
	s6-8	Superior 6-8 Transitional Area
	SFL	Superior Frontal Language Area
Premotor Cortex	55b	Area 55b
	6a	Area 6 anterior
	6d	Dorsal area 6
	6r	Rostral Area 6
	6v	Ventral Area 6
	FEF	Frontal Eye Fields
	PEF	Premotor Eye Field
Orbital and Polar Frontal Cortex	10d	Area 10d
	10pp	Polar 10p
	11l	Area 11l
	13l	Area 13l
	47m	Area 47m
	47s	Area 47s

	a10p	Area anterior 10p
	a47r	Area anterior 47r
	OFC	Orbital Frontal Complex
	p10p	Area posterior 10p
	pOFC	posterior OFC Complex
Inferior Frontal Cortex	44	Area 44
	45	Area 45
	47l	Area 47l (47 lateral)
	IFJa	Area IFJa
	IFJp	Area IFJp
	IFSa	Area IFSa
	IFSp	Area IFSp
	p47r	Area posterior 47r
Posterior Opercular Cortex	43	Area 43
	FOP1	Frontal Opercular Area 1
	OP1	Area OP1/SII
	OP2-3	Area OP2-3/VS
	OP4	Area OP4/PV
	PFcm	Area PFcm